Electronic Supplementary Information (ESI) for RSC

Functional Transformation of Four-Bladed Rylene Propellers Utilizing Non-Metal and d^8 Metal Core Shifting Strategy: Significant Impact on Photovoltaic Performance and Electrocatalytic Hydrogen Evolution Activity

Jianhua Han, Wenwen Shi, Xunchang Wang, Jingwen Cai, Xinyu Hao, Jingying Shi, Xichang Bao and Renqiang Yang**

Table of Contents

1. Materials and Measurements

The synthetic procedures were performed under argon atmosphere. Commercial chemicals (from Sigma-Aldrich, Aladdin Chemical and Energy Chemical) were used as received. Monobrominated PDI (**1**) and 1,2-bis(4-(4,4,5,5-tetramethyl-1,3,2-dioxaborolan-2-yl)phenyl) ethane-1,2-dione (**2**) were prepared according to literature procedures[1, 2]. Pt-PH were prepared as literature procedures.[3] ^{1}H NMR (600 MHz) and ^{13}C NMR (150 MHz) spectra were recorded in deuterated solvents on Bruker AVANCE III 600 MHz spectrometer at 298 K. Chemical shifts are in ppm downfield from tetramethylsilane (TMS) reference using the residual protonated solvent as an internal standard. High-resolution mass spectra (HRMS) and matrix-assisted laser desorption ionization time-of-flight mass spectroscopy (MALDI-TOF-MS) were determined on a ultraflextreme MALDI-TOF/TOF (Bruker Corp.).

Optical absorption spectra were recorded on a Hitachi U-4100 UV-Vis scanning spectrophotometer. Cyclic voltammetry (CV) measurements were performed on a CHI660D electrochemical workstation, equipped with a three-electrode cell consisting of a platinum working electrode, a saturated calomel electrode (SCE) as reference electrode and a platinum wire counter electrode. CV measurements were carried out in anhydrous acetonitrile containing 0.1 M n-Bu_4NPF_6 as a supporting electrolyte under an argon atmosphere at a scan rate of 100 mV s^{-1} assuming that the absolute energy level of Fc/Fc^+ was -4.80 eV. Thin films were deposited from $CHCl_3$ solution onto the working electrodes. Grazing incidence wide-angle X-ray scattering (GIWAXS) patterns were acquired by beamline BL16B1 (Shanghai Synchrotron Radiation Facility). The X-ray wavelength was 0.124 nm (E = 10 keV) and the incidence angle was set to 0.12. Transmission electron microscopy (TEM) images were obtained by using a HITACHI H-7650 electron microscope with an acceleration voltage of 100 kV. Atomic force microscopy (AFM) images were obtained using Agilent 5400 scanning probe microscope in tapping mode with Mikro Masch NSC-15 AFM tips. Photoluminescence (PL) and Transient photoluminescence spectra were taken on an Edinburgh Instrument FLS1000. Ultraviolet photoelectron spectroscopy(UPS) were performed on the PHI5000 VersaProbe III (Scanning ESCA Microprobe) SCA (Spherical Analyzer). The gas discharge lamp was used for UPS, with helium gas admitted and the HeI (21.22 eV) emission line employed. Thermal gravimetric analyses (TGA) were carried out on a Mettler TGA/SDTA851 thermogravimetric analysis instrument (Mettler-Toledo) with four heating rates 20 °C/min from 30 to 800 °C under nitrogen atmosphere. Differential scanning calorimeter (DSC) was recorded on a Mettler DSC822 (Mettler-Toledo) in flowing nitrogen with a heating rate of 10 °C min^{-1}. Elemental analysis was estimated using a Vario EL CUBE (Elementar Ltd., Germany).

Density functional theory (DFT) calculations were performed using the hybrid BLYP35 function to obtain the optimal 3D molecular geometries[4, 5]. In order to facilitate the calculation, we used methyl to replace branched alkyl chains. For the valence and core electrons of metal atoms and S atoms, the double-ξ quality LANL2DZ basis set and the Los Alamos effective core potentials were used. For all other atoms, the 6-31G(d) basis set was used.

The DFT calculations were also conducted for the hydrogen binding energy calculated from metal active sites according to the literatures [6-9]. A Perdew-Burke-Ernzerhof (PBE) functional was used to treat the electron exchange correlation (EEC) interaction. For the valence and core electrons of metal atoms and S atoms, the double-ξ quality LANL2DZ basis set and the Los Alamos effective core potentials were used. For all other atoms, the 6-311+G(d,p) basis set was used. In order to facilitate the calculation, the PDI moiety was replaced by hydrogen atom. To consider the influence of van der Waals interaction, the semi-empirical DFT-D3 force-field approach was applied. The Gibb's free energies for hydrogen absorption $|\Delta G_{H^*}|$ were calculated from the given equation: $\Delta G_{H^*} = \Delta E_{H^*} + \Delta ZPE - T\Delta S$, where the symbols represent the binding energy (ΔE), the change in zero-point energy (ΔE_{ZPE}), Temperature (T), and the entropy change (ΔS) of the system, respectively. We adopted the approximation that the vibrational entropy of hydrogen in the adsorbed state is negligible, in which case $\Delta S_H \approx S_{H^*} - 1/2(S_{H2}) \approx -1/2(S_{H2})$, where S_{H2} is the entropy of H_2(g) at standard conditions. Herein, the calculated TS_{H2} is 0.40 eV for H_2 at 298.15 K and 1 atm, which is consistent with the reference value of 0.41 eV at 300 K and 1 atm.[8]

Photovoltaic devices were fabricated with a conventional device structure of ITO/PEDOT:PSS/polymer:PDI propellers/PDINO/Al. The patterned ITO glass was pre-cleaned in an ultrasonic bath of acetone and isopropyl alcohol and treated in an ultraviolet-ozone chamber (PREEN II-862) for 6 min. Then a thin layer (about 30 nm) of PEDOT:PSS was spin-coated onto the ITO glass at 4000 rpm and baked at 160 ^{o}C for 20 min. Solutions of polymer/PDI propellers in chlorobenzene (24 mg/mL, total concentration) were stirred overnight and spin-coating on the PEDOT:PSS layer to form the active layer about 100±20 nm. The thickness of the active layer was measured using a Veeco Dektak 150 profilometer. Then PDINO solution (in CH_3OH, 1 mg/mL) was spin-coating at 3000 rpm for 15 s to form the electron transfer layer. Finally, Al (300 nm) metal electrode was thermal evaporated under about 5×10^{-4} Pa and the device area was 0.1 cm^2 defined by shadow mask. The current density-voltage (*J*-*V*) characteristics were recorded with a Keithley 2400 source measurement unit under simulated 100 mW cm^{-2} irradiation from a Newport solar simulator. The external quantum

efficiencies (EQEs) were analysed using a certified Newport incident photon conversion efficiency measurement system. The hole mobility and electron mobility were measured by space-charge-limited current (SCLC) method with a device configuration of ITO/PEDOT:PSS/active layer/MoO_3/Al and ITO/ZnO/active layer/PDINO/Al structure, respectively. The SCLC is described by the Mott-Gurney law: $J = 9\varepsilon\mu V^2/(8L^3)$, where ε represents the dielectric constant of the metal, and μ is the carrier mobility, *V* is the voltage drop across the device and L is the thickness of the active layer.

Hydrogen evolution reaction measurements were conducted in a three-electrode system with a potentiostat (CH Instruments 660D potentiostat). The working electrode was a glassy carbon electrode (GCE, geometric area of 0.070 cm^2). The synthesized six four-bladed PDI propeller samples were attached onto the glassy carbon electrode (GCE): 2 mg of each sample and 10 μl of 5 wt% Nafion solution were dispersed in 200 μl of a water/ethanol (1:3 v/v) mixed solvent and sonicated for 30 min, and then 10 μl of the homogeneous ink was dropped onto the GCE. The dried hybrid catalysts/GCE was used as working electrodes. A graphite rod and an SCE were used as counter and reference electrodes, respectively. The electrolyte solution was 0.5 M H_2SO_4 (pH=0). The measured potentials versus SCE were converted to the reversible hydrogen electrode (RHE) scale according to the Nernst equation: $V_{RHE} = V_{SCE} + 0.242 + 0.059 \times pH$. The linear sweep voltammogram tests were performed at a scan rate of 10 mV s^{-1}. The Tafel slopes were determined by fitting the linear portion of the plot starting from the onset potential (to the end point which does not significantly deviate from the slope line). The Tafel slopes were calculated by fitting to the Tafel equation: $\eta = b\log j + c$, where *b* is the Tafel slope, *j* is the current density and *c* is the intercept relative to j_0.

2. Synthetic Details

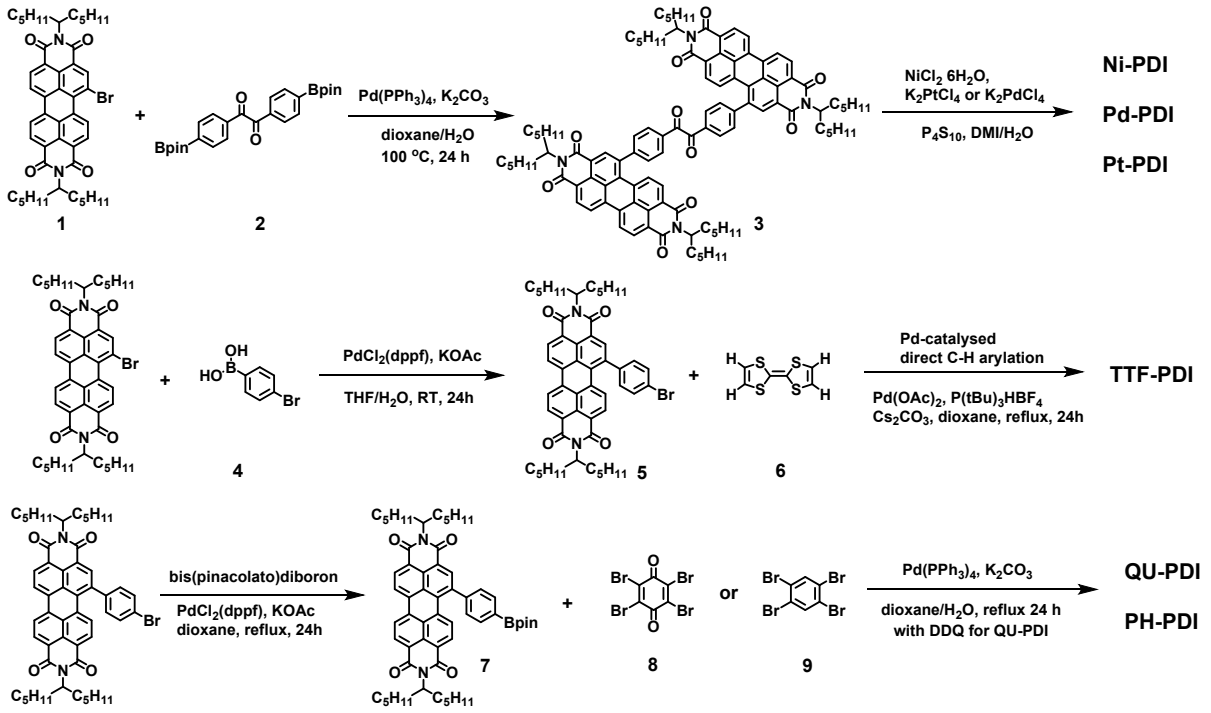

Figure S1. The synthetic route of six PDI propellers.

Compound 3: A Schlenk flask was charged with 1,2-bis(4-(4,4,5,5-tetramethyl-1,3,2-dioxaborolan-2-yl)phenyl)ethane-1,2-dione (**2**) (1.0 eq.), corresponding monobrominated PDI (**1**) (2.4 eq.), 1,4-dioxane (20 mL/2.0 g of **1**) and 4 mL K_2CO_3 aqueous solution (2M). The mixture was degassed with argon for 15 min. $Pd(PPh_3)_4$ (0.12 eq.) was added under an argon atmosphere. The mixture was refluxed for 48 h and then cooled down to room temperature. The cooled mixture was poured into 1M HCl aqueous solution (1000 mL) and stirred for 2 h. The precipitate was collected by vacuum filtration, washed with water and CH_3OH, dried, and purified by column chromatography on silica gel, eluted with petroleum ether/CH_2Cl_2 (1:1 v/v) to afford **3** as dark red solids, yield: 76%. ^1H NMR (600 MHz, $CDCl_3$) δ: 8.75-8.64 (m, 4H), 8.57 (d, 1H), 8.22 (t, 3H), 7.86 (d, 1H), 7.76 (d, 2H), 5.17 (m, 2H), 2.26-2.14 (m, 4H), 1.86-1.78 (m, 4H), 1.24 (m, 24H), 0.84-0.79 (m, 12H). MS (MALDI-TOF) calc. for [$C_{106}H_{114}N_4O_{10}$]:1603.0. Found for 1603.7.

Compound Ni-PDI: Under argon atmosphere, of heating at 110 °C a mixture of **3** (200 mg, 1.0 eq.) and phosphorus pentasulfide (554 mg, 10.0 eq.) in 10 mL of 1,3-dimethyl-2-imidazolidinone (DMI) for 3 h. The reaction mixture was cooled to 60 °C. A solution of nickel chloride hexahydrate NiCl•$6H_2O$ (15 mg, 0.5 eq.) in water (1 mL) was added to the reaction mixture and reacted to 90 °C for 2 h in air. To the resulting mixture was added ethanol and the precipitate was filtered, washed with ethanol and dried under vacuum. The purification of products was carried out by chromatography on silica gel,

eluting with CH_2Cl_2. Dark red solids were obtained by slow diffusion of MeOH on a solution of the product in CH_2Cl_2, yield: 19%. ^{1}H NMR (600 MHz, $CDCl_3$) δ: 8.73-8.58 (m, 20H), 8.17 (s, 4H), 7.98 (d, 4H), 7.77 (d, 8H), 7.62 (d, 8H), 5.20-5.00 (m, 8H), 2.21 (s, 16H), 1.82-1.63 (m, 16H), 1.29-1.15 (m, 96H), 0.78 (d, *J* = 18.7 Hz, 48H). ^{13}C NMR (150 MHz, $CDCl_3$) δ:180.92 (s), 164.90-164.72 (m), 163.83-163.33 (m), 143.76 (s), 141.47 (s), 140.78 (s), 134.52 (d), 131.04 (s), 130.31 (s), 129.30 (d), 128.80 (s), 128.28 (s), 127.67 (s), 123.71 (s), 122.93 (s), 54.90 (s), 32.38 (d), 31.81 (d), 29.82 (s), 26.68 (d), 22.64 (d), 14.14 (d). HRMS(MALDI-TOF) calc. for $[C_{212}H_{228}N_8NiO_{16}S_4\text{-}H]^-$:3328.5498. Found for 3328.5507. Elemental analysis (calculated, found for $C_{212}H_{228}N_8NiO_{16}S_4$): C (76.44, 76.91), H (6.90, 6.17), N (3.36, 2.81).

Compound Pd-PDI: Under argon atmosphere, of heating at 110 °C a mixture of **3** (200 mg, 1.0 eq.) and phosphorus pentasulfide (554 mg, 10.0 eq.) in 10 mL of 1,3-dimethyl-2-imidazolidinone (DMI) for 3 h. The reaction mixture was cooled to 60 °C. A solution of potassium palladium(II) chloride K_2PdCl_4 (20 mg, 0.5 eq.) in water (1 mL) was added to the reaction mixture and reacted to 90 °C for 2 h in air. To the resulting mixture was added ethanol and the precipitate was filtered, washed with ethanol and dried under vacuum. The purification of products was carried out by chromatography on silica gel, eluting with CH_2Cl_2. Dark red solids were obtained by slow diffusion of MeOH on a solution of the product in CH_2Cl_2, yield: 9%. ^{1}H NMR (600 MHz, $CDCl_3$) δ: 8.62 (dd, 20H), 8.14 (s, 4H), 7.94 (d, 4H), 7.65 (dd, 16H), 5.06 (m, 8H), 2.21 (d, 16H), 1.81 (m, 16H), 1.22 (m, 96H), 0.81-0.71 (m, 48H). ^{13}C NMR (150 MHz, $CDCl_3$) δ: 182.02(s), 164.83 (d), 163.77 (d), 143.90 (s), 142.34 (s), 140.69 (s), 134.99 (s), 134.51 (d), 129.96 (dd), 129.31 (s), 129.21 (d), 129.17-128.77(m), 127.97 (d), 127.67 (s), 123.81-123.56 (m), 123.18 -122.88 (m), 54.87 (d), 32.38 (d), 31.78 (d), 29.83 (s), 26.68 (d), 22.69 (t), 14.20 (d). HRMS (MALDI-TOF) calc. for $[C_{212}H_{228}N_8PdO_{16}S_4\text{-}H]^-$:3375.5196. Found for 3375.5233. Elemental analysis (calculated, found for $C_{212}H_{228}N_8PdO_{16}S_4$): C (75.36, 74.98), H (6.80, 5.94), N (3.32, 3.11).

Compound Pt-PDI: Under argon atmosphere, of heating at 110 °C a mixture of **3** (200 mg, 1.0 eq.) and phosphorus pentasulfide (554 mg, 10.0 eq.) in 10 mL of 1,3-dimethyl-2-imidazolidinone (DMI) for 3 h. The reaction mixture was cooled to 60 °C. A solution of potassium tetrachloroplatinate(II) K_2PtCl_4 (20 mg, 0.5 eq.) in water (1 mL) was added to the reaction mixture and reacted to 90 °C for 2 h in air. To the resulting mixture was added ethanol and the precipitate was filtered, washed with ethanol and dried under vacuum. The purification of products was carried out by chromatography on silica gel,

eluting with CH_2Cl_2. Dark red solids were obtained by slow diffusion of MeOH on a solution of the product in CH_2Cl_2, yield: 23%. ^{1}H NMR (600 MHz, $CDCl_3$) δ: 8.70-8.54 (m, 20H), 8.20-8.06 (m, 4H), 7.96 (d,4H), 7.65 (dd, 16H), 5.17-4.97 (m, 8H), 2.26-2.05 (m, 16H), 1.82 (d, 16H), 1.25 (s, 96H), 0.84-0.74 (m, 48H). ^{13}C NMR (150 MHz, $CDCl_3$) δ: 177.23 (s), 164.97-164.73 (m), 163.86-163.65 (m), 143.72 (s), 141.47 (s), 140.74 (s), 135.01 (s), 134.61- 134.28 (m), 133.13-132.80 (m), 131.82-131.54 (m), 131.14 (s), 130.29 (s), 129.31 (s), 129.16 (s), 128.80 (s), 128.27 (s), 127.68 (s), 123.71 (s), 122.93 (s), 54.90 (s), 32.44 (s), 31.82 (d), 29.83 (s), 26.68 (d), 22.65 (d), 14.14 (d). HRMS (MALDI-TOF) calc. for $[C_{212}H_{228}N_8PtO_{16}S_4\text{-}H]^-$:3464.5804. Found for 3464.5738. Elemental analysis (calculated, found for $C_{212}H_{228}N_8PtO_{16}S_4$): C (73.43, 72.73), H (6.63, 6.56), N (3.23, 2.82).

Compound 5[10]: monobrominated PDI (**1**) (100 mg, 1.0 eq.) and 4-bromobenzeneboronic acid (130 mg, 5 eq.), Pd(dppf)Cl_2 (9 mg, 0.1 eq.) were added into a Schlenk flask (50 mL). The mixture was degassed and charged with argon for three times. Then oxygen-free THF (5 mL) and KOAc aqueous solution (2 M, 1 mL) were added into the flask. The mixture was reacted for 24 h at 25 °C and then poured into 1M HCl aqueous solution (1000 mL) and stirred for 2 h. The precipitate was collected by vacuum filtration, washed with water and CH_3OH, dried, and purified by column chromatography on silica gel, eluted with petroleum ether/CH_2Cl_2 (1:1 v/v) to afford **5** as dark red solids, yield: 89%. ^{1}H NMR (600 MHz, $CDCl_3$) δ: 8.74-8.59 (m, 4H), 8.58-8.44 (m, 1H), 8.25-8.07 (m, 1H), 7.86 (d, 1H), 7.67 (d, 2H), 7.39 (d, 2H), 5.25-5.08 (m, 2H), 2.29-2.18 (m, 4H), 1.87-1.78 (m, 4H), 1.33-1.23 (m, 24H), 0.83 (m, 12H). HRMS (MALDI-TOF) calc. for $[C_{52}H_{57}BrN_2O_4]$:852.3502. Found for 852.3527.

Compound TTF-PDI[11]: $Pd(OAc)_2$ (1 mg, 0.3 eq.), P*t*Bu_3•HBF_4 (5 mg, 0.9 eq.), and Cs_2CO_3 (36 mg, 6.0 eq.) were placed in a 25-mL reaction flask under nitrogen. Dioxane (2.5 mL) was added and the mixture was stirred for 10 min with heating. A solution of tetrathiafulvalene (4 mg, 1.0 eq.) and compound **5** (79 mg, 5.0 eq.) in dioxane (2.5 mL) was added. The mixture was heated at reflux for 24 h. The organic compounds were extracted with dichloromethane three times. The combined organic part was washed with brine, dried over anhydrous Na_2SO_4, and concentrated in vacuo. The residue was purified by gel permeation chromatography with chloroform as an eluent to afford TTF-PDI as a dark red solid, yield: 43%. ^{1}H NMR (600 MHz, $CDCl_3$) δ: 8.62 (dd, 20H), 8.14 (d,4H), 7.90 (d, 4H), 7.56 (d, 16H), 5.22-4.96 (m, 8H), 2.21 (s, 16H), 1.82 (s, 16H), 1.28-1.12 (m, 96H), 0.78 (m, 48H). ^{13}C NMR (150 MHz, $CDCl_3$) δ: 164.99 (s), 164.94-164.68 (m), 163.75 (d), 140.73 (s), 134.51 (s), 133.07 (s),

131.18 (s), 130.19 (s), 129.56-129.11 (m), 128.75 (s), 128.51-128.22 (m), 127.92 (d), 123.80-123.51 (m), 123.05 (s), 122.89 (s), 58.58 (s), 54.87 (s), 31.97 (dd), 26.93-26.04 (m), 22.63 (d), 18.57 (s), 14.13 (d). HRMS (MALDI-TOF) calc. for $[C_{214}H_{228}N_8O_{16}S_4\text{-}H]^{-}$:3296.4580. Found for 3296.5870. Elemental analysis (calculated, found for $C_{214}H_{228}N_8O_{16}S_4$): C (77.97, 77.49), H (6.97, 6.31), N (3.40, 3.14).

Compound 7: Compound **5** (854 mg, 1 eq.) and bis(pinacolato)diboron (757 mg, 2.0 eq.), $Pd(dppf)Cl_2$ (109 mg, 0.1 eq.) , AcK (512 mg, 3.5 eq.) were added into a Schlenk flask (50 mL). The mixture was degassed and charged with argon for three times. Then oxygen-free and super-dry dioxane (25 mL) was added into the flask, the mixture was reacted for 24 h at 100 °C. After cooling to room temperature, solvent was removed under reduced pressure. The crude product was purified by column chromatography on a fast silica gel and eluted with CH_2Cl_2, then washed with petroleum ether to afford compound **7** as red solids, yield: 83%.^{1}H NMR (600 MHz, $CDCl_3$) δ: 8.63 (dd, 5H), 8.20-8.04 (m, 1H), 7.95 (d, 2H), 7.82 (d, 1H), 7.54 (dd, 2H), 5.23-5.10 (m, 2H), 2.24 (dd, 4H), 1.87-1.76 (m, 4H), 1.42 (s, 12H), 1.26 (s, 24H), 0.84-0.79 (m, 12H). HRMS (HR-MALDI-TOF) calc. for $[C_{58}H_{69}BN_2O_6]$: 900.5249 Found for 900.5297.

Compound QU-PDI[12]: To a mixture of compound **7** (150 mg, 4.5 eq.), **8** (16 mg, 1.0 eq.), $Pd(PPh_3)_4$ (20 mol %) were added dioxane (10 mL) and aqueous K_2CO_3 (2 M, 10.0 eq.) under argon atmosphere. The reaction mixture was refluxed for 24 h. The reaction mixture was allowed to cool to 20 °C and then ice-cooled water (8 mL) was added. After stirring for 15 min, the mixture was extracted with dichloromethane. The organic layer was washed with brine, dried (Na_2SO_4), filtered, and concentrated in vacuo. The crude product was purified by flash column chromatography (silica gel, CH_2Cl_2). A benzene solution (8.5 mL) of DDQ was stirred at 20 °C for 24 h. The reaction mixture was filtered, dried (Na_2SO_4), filtered and the filtrate was concentrated. The residue was purified by chromatography (silica gel, CH_2Cl_2) to give QU-PDI as a dark red solid, yield: 15%. ^{1}H NMR (600 MHz, $CDCl_3$) δ: 8.83-8.46 (m, 20H), 8.18 (dd, 4H), 8.00 (d, 4H), 7.37 (d, 8H), 7.03 (d, 8H), 5.24-5.06 (m, 8H), 2.25 (s, 16H), 1.85 (d, 16H), 1.31-1.21 (m, 96H), 0.82 (m, 48H). ^{13}C NMR (150 MHz, $CDCl_3$) δ: 185.64(s), 163.54 (dd), 142.33 (s), 138.97-138.77 (m), 132.36 (s), 131.31 (s), 128.93 (s), 128.62 (s), 128.04 (d), 126.92 (s), 123.64 (s), 122.91 (s), 120.92 (s), 54.84 (s), 32.35 (d), 31.82 (d), 29.77 (s), 26.72 (d), 22.66 (s), 14.14 (s). HRMS (MALDI-TOF) calc. for $[C_{214}H_{228}N_8O_{18}+H]^{+}$:3199.7239. Found for 3199.7348.

Elemental analysis (calculated, found for $C_{214}H_{228}N_8O_{18}$): C (80.32, 80.36), H (7.18, 6.89), N (3.50, 2.66).

Coumpound PH-PDI: To a mixture of compound **7** (150 mg, 4.5 eq.), 9 (15 mg, 1.0 eq.), $Pd(PPh_3)_4$ (20 mol %) were added dioxane (10 mL) and aqueous K_2CO_3 (2 M, 10.0 eq.) under argon atmosphere. The reaction mixture was refluxed for 24 h. The reaction mixture was allowed to cool to 20 °C and then ice-cooled water (8 mL) was added. After stirring for 15 min, the mixture was extracted with dichloromethane. The organic layer was washed with brine, dried (Na_2SO_4), filtered, and concentrated in vacuo. The crude product was purified by flash column chromatography (silica gel, CH_2Cl_2) to give PH-PDI as a dark red solid, yield: 42%. ^{1}H NMR (600 MHz, $CDCl_3$) δ: 8.79-8.48 (m, 20H), 8.17-8.07 (m, 4H), 8.01 (s, 4H), 7.85 (d, 4H), 7.72-7.49 (m, 16H), 5.19-4.96 (m, 8H), 2.32- 2.07 (m, 16H), 1.81 (dd, 16H), 1.19 (m, 96H), 0.77 (m, 48H). ^{13}C NMR (150 MHz, $CDCl_3$) δ: 163.69 (dd), 140.54 (d), 140.20 (d), 138.40 (s), 134.39 (s), 133.79 (ddd), 133.45 (dd), 131.72-131.55 (m), 130.90 (s), 130.62 (ddd), 129.63 (dd), 129.19 (s), 128.96 (dd), 128.17 (d), 127.84-127.46 (m), 127.46-126.85 (m), 126.55 (t), 122.48 (d), 121.65 (s), 54.48-53.46 (m), 31.69-30.46 (m), 30.45-29.98 (m), 28.67 (s), 25.53 (dd), 21.50 (t), 12.99 (t). HRMS (MALDI-TOF) calc. for $[C_{214}H_{230}N_8O_{16}+H]^+$:3169.7497. Found for 3169.7053. Elemental analysis (calculated, found for $C_{214}H_{230}N_8O_{16}$): C (81.08, 80.93), H (7.31, 7.11), N (3.53, 3.72).

3. ^{1}H NMR and ^{13}C NMR Spectra of Compounds

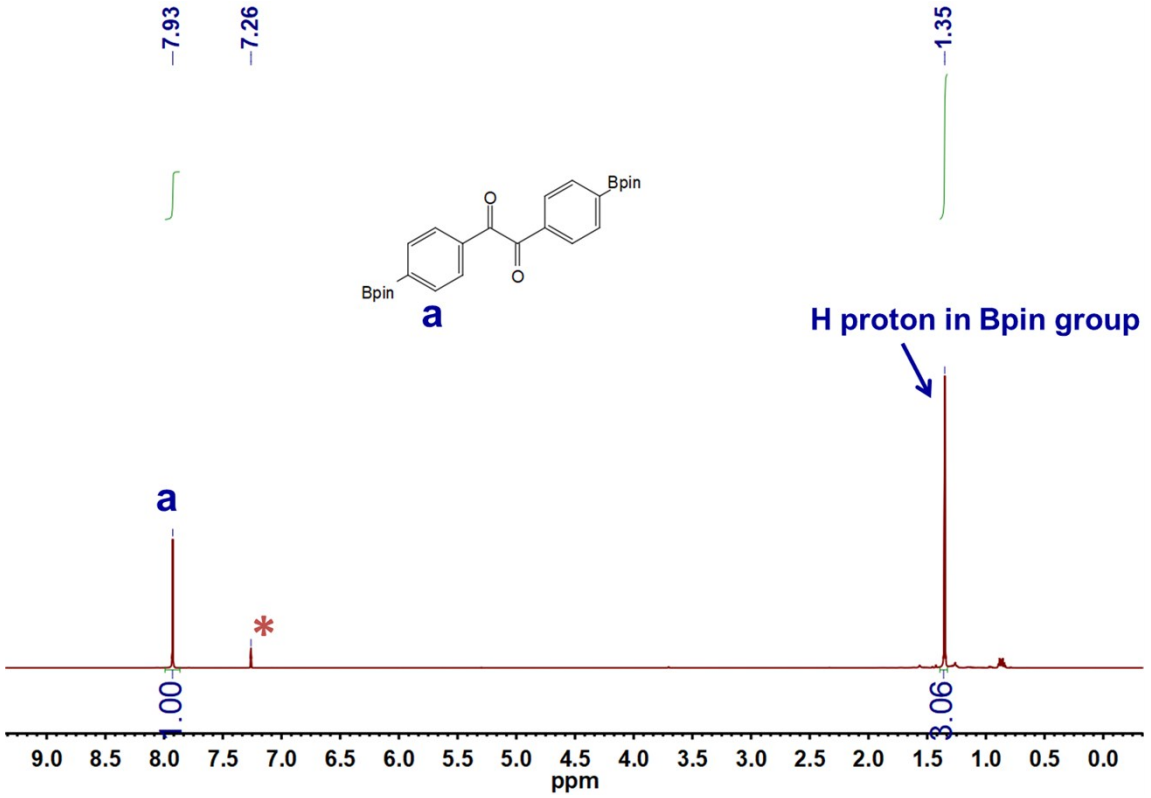

Figure S2. ^{1}H NMR spectrum of compound **2**.

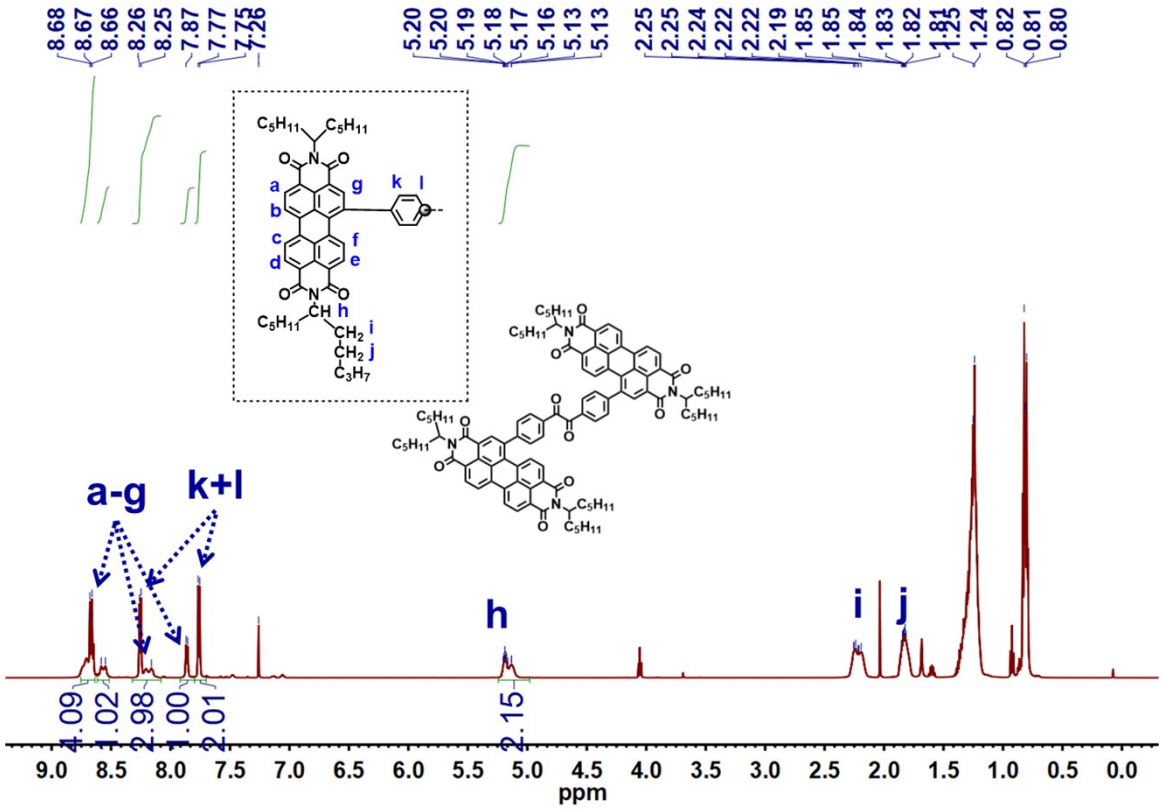

Figure S3. ^{1}H NMR spectrum of compound **3**.

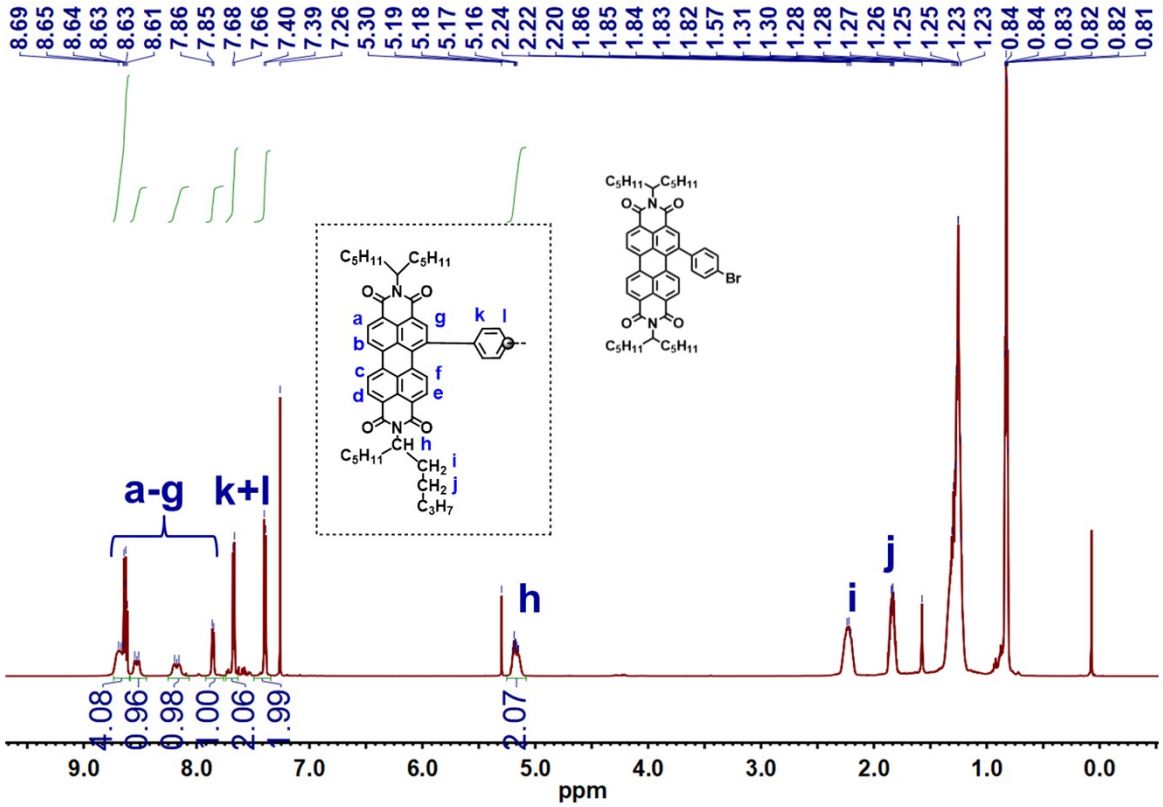

Figure S4. ^{1}H NMR spectrum of compound **5**.

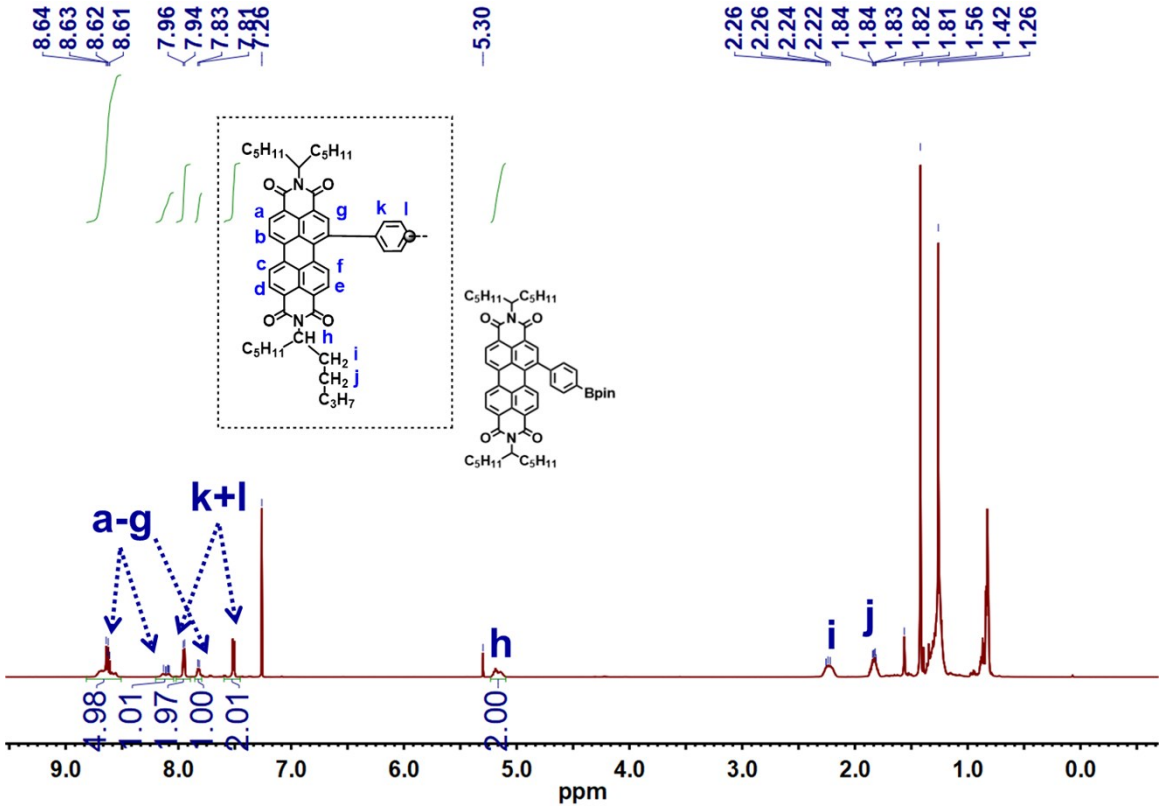

Figure S5. ^{1}H NMR spectrum of compound **7**.

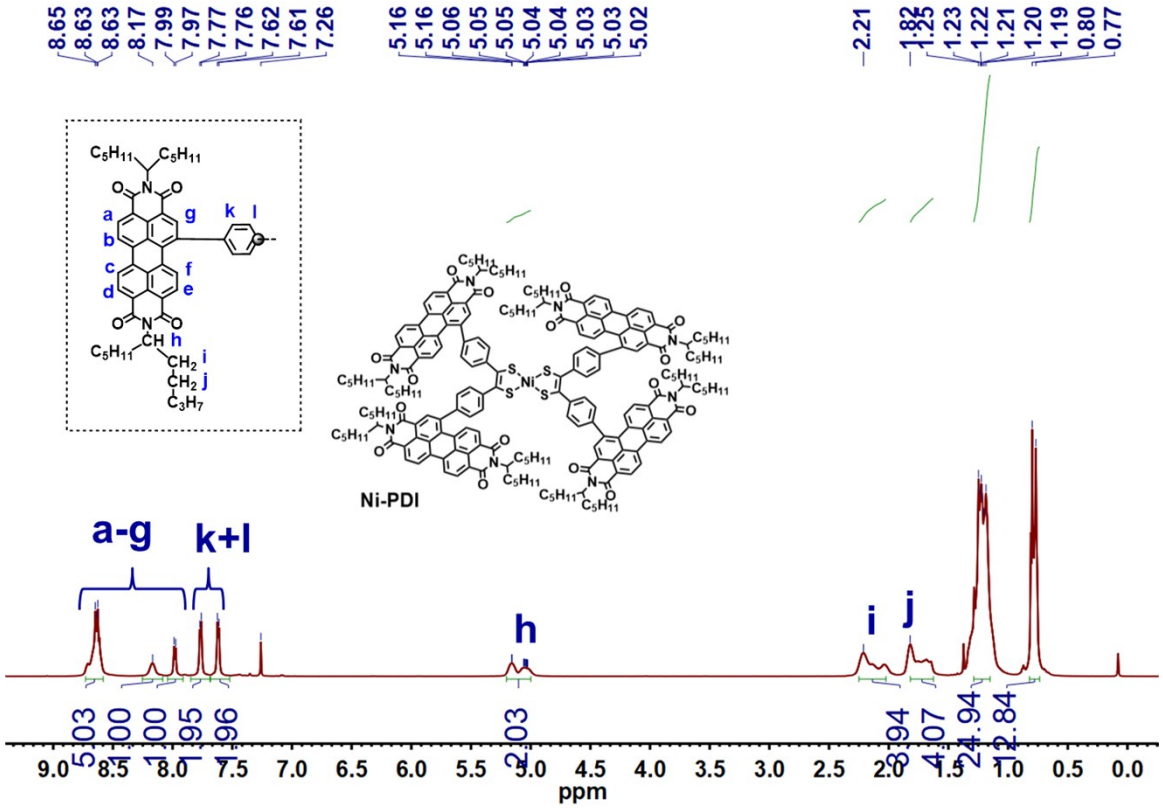

Figure S6. ^{1}H NMR spectrum of compound **Ni-PDI**.

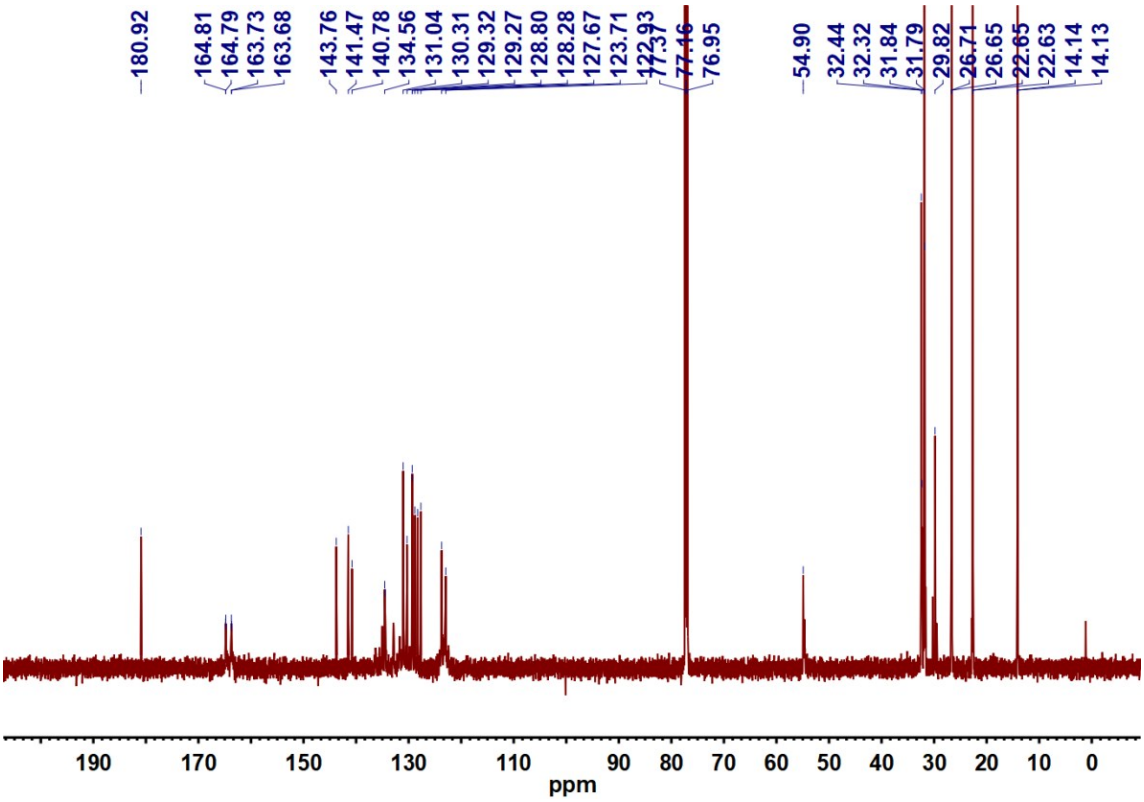

Figure S7. ^{13}C NMR spectrum of compound **Ni-PDI**.

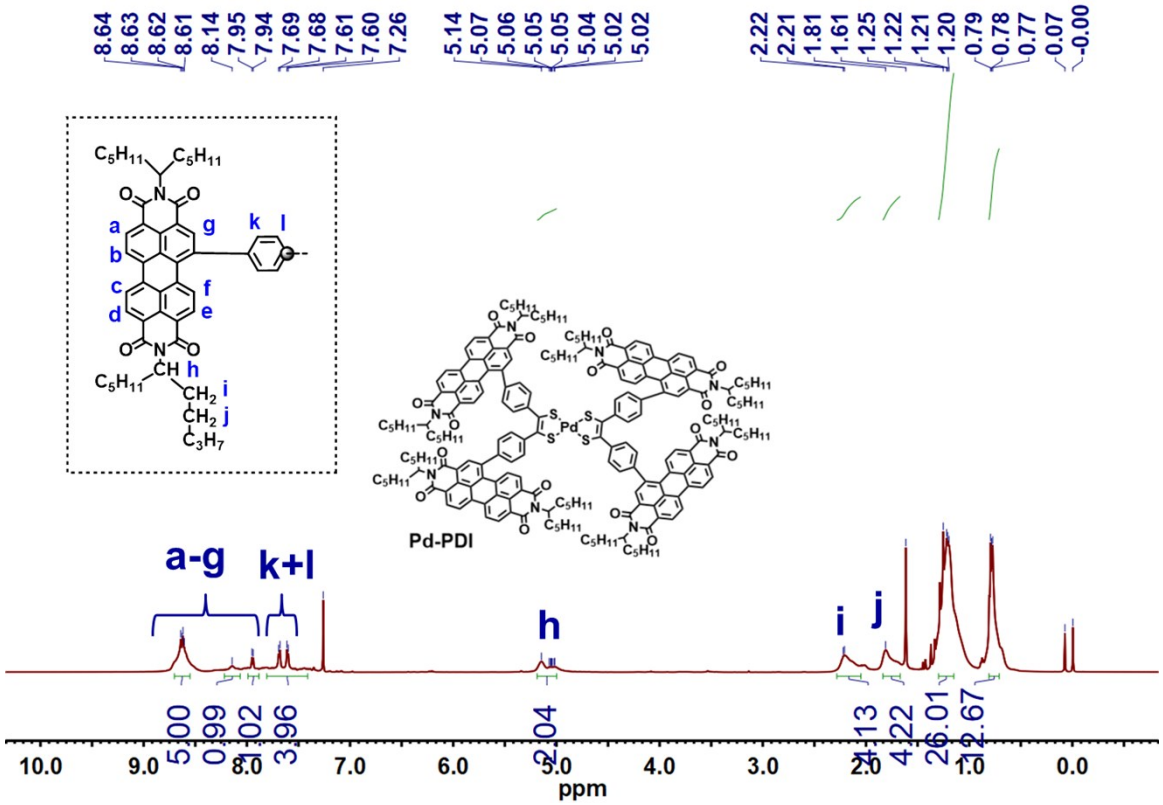

Figure S8. ^{1}H NMR spectrum of compound **Pd-PDI**.

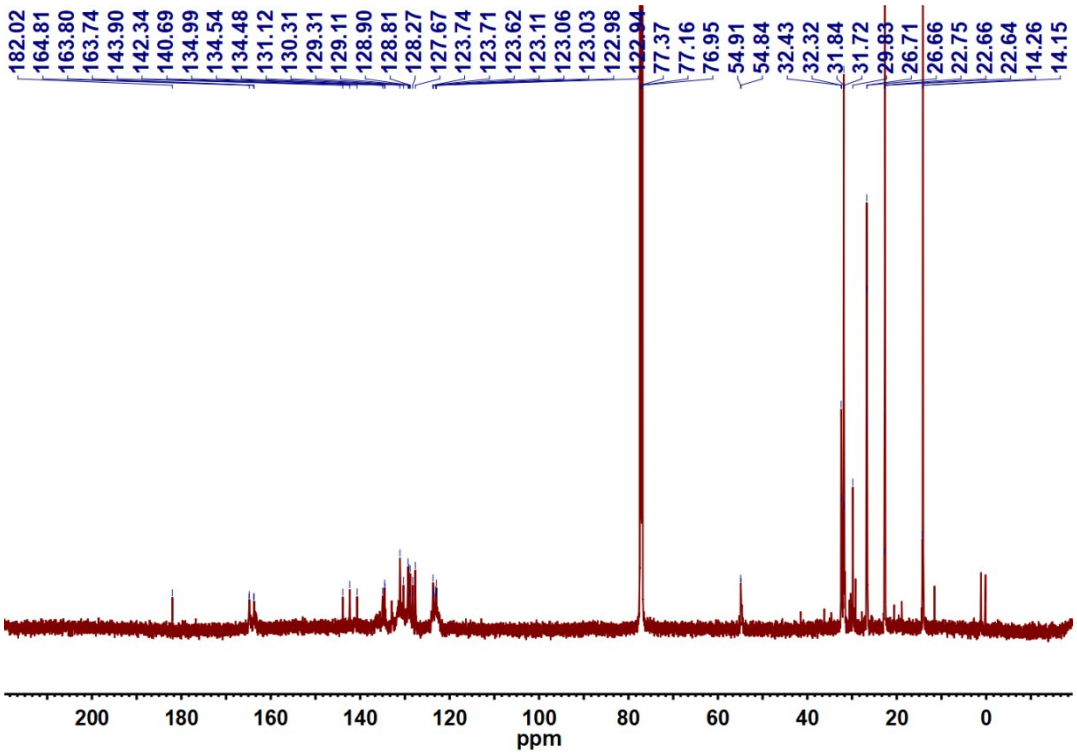

Figure S9. ^{13}C NMR spectrum of compound **Pd-PDI**.

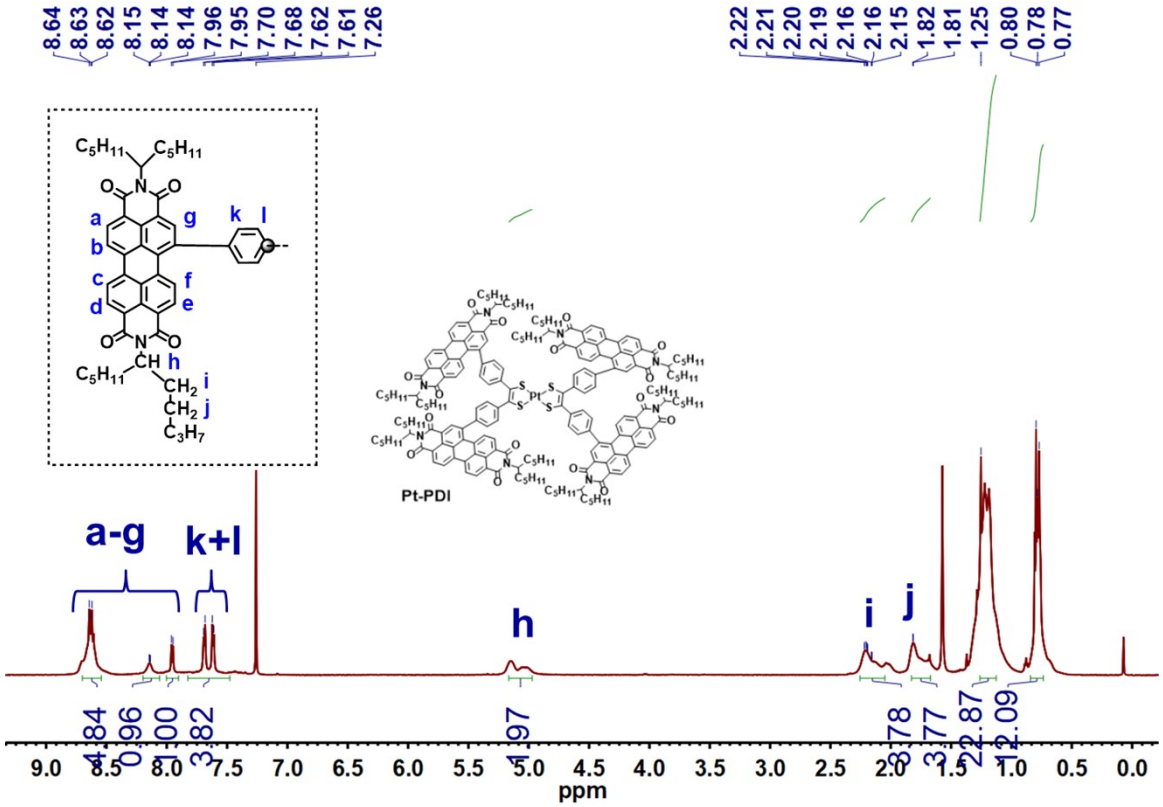

Figure S10. ^{1}H NMR spectrum of compound **Pt-PDI**.

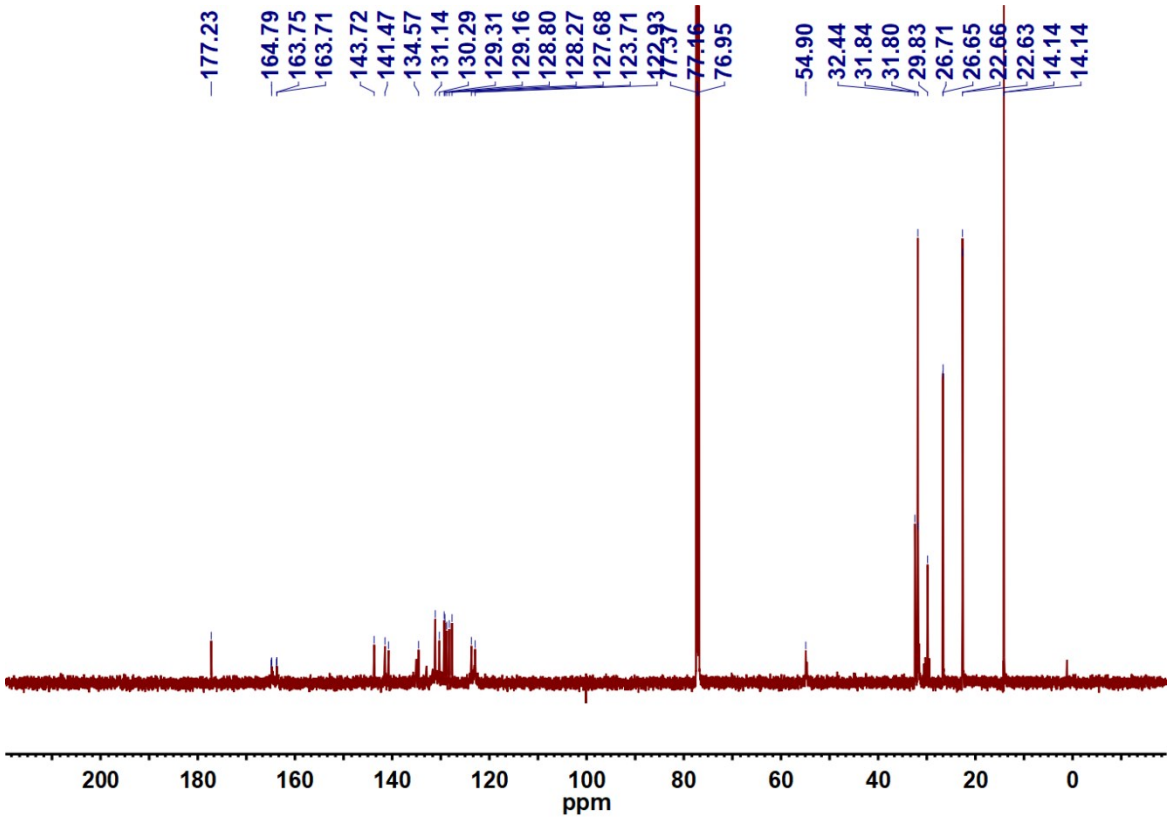

Figure S11. ^{13}C NMR spectrum of compound **Pt-PDI**.

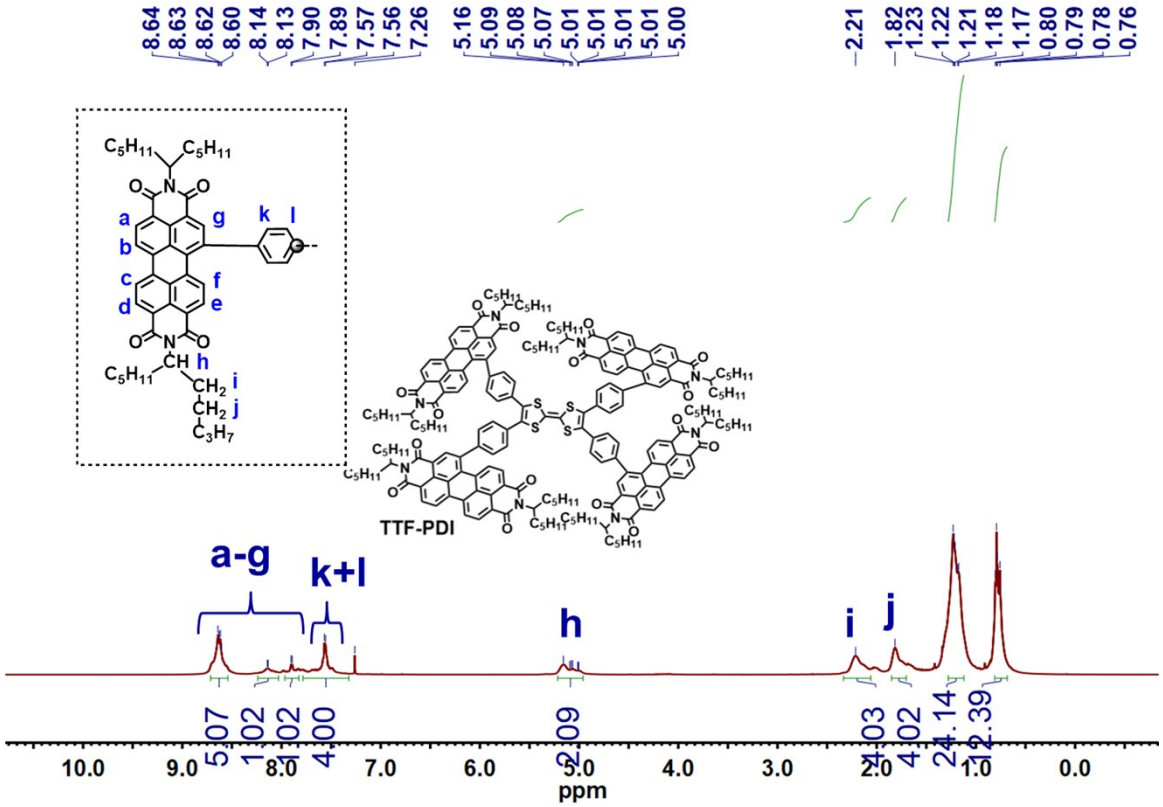

Figure S12. ^{1}H NMR spectrum of compound **TTF-PDI**.

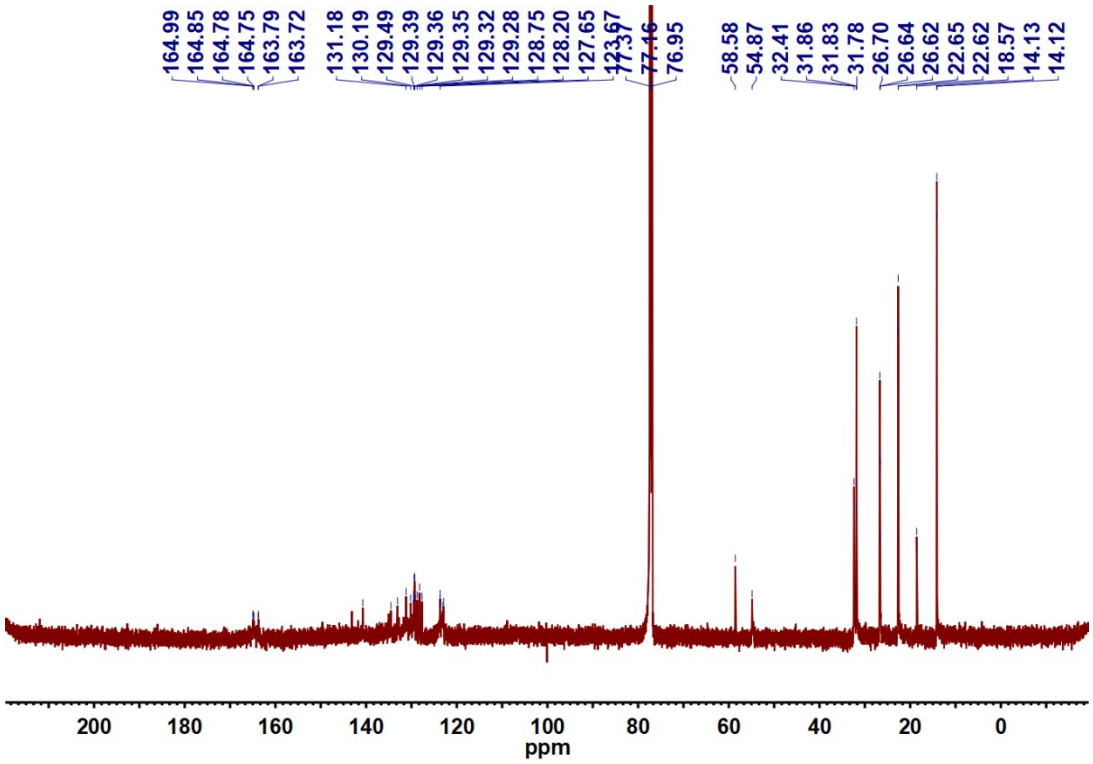

Figure S13. ^{13}C NMR spectrum of compound **TTF-PDI**.

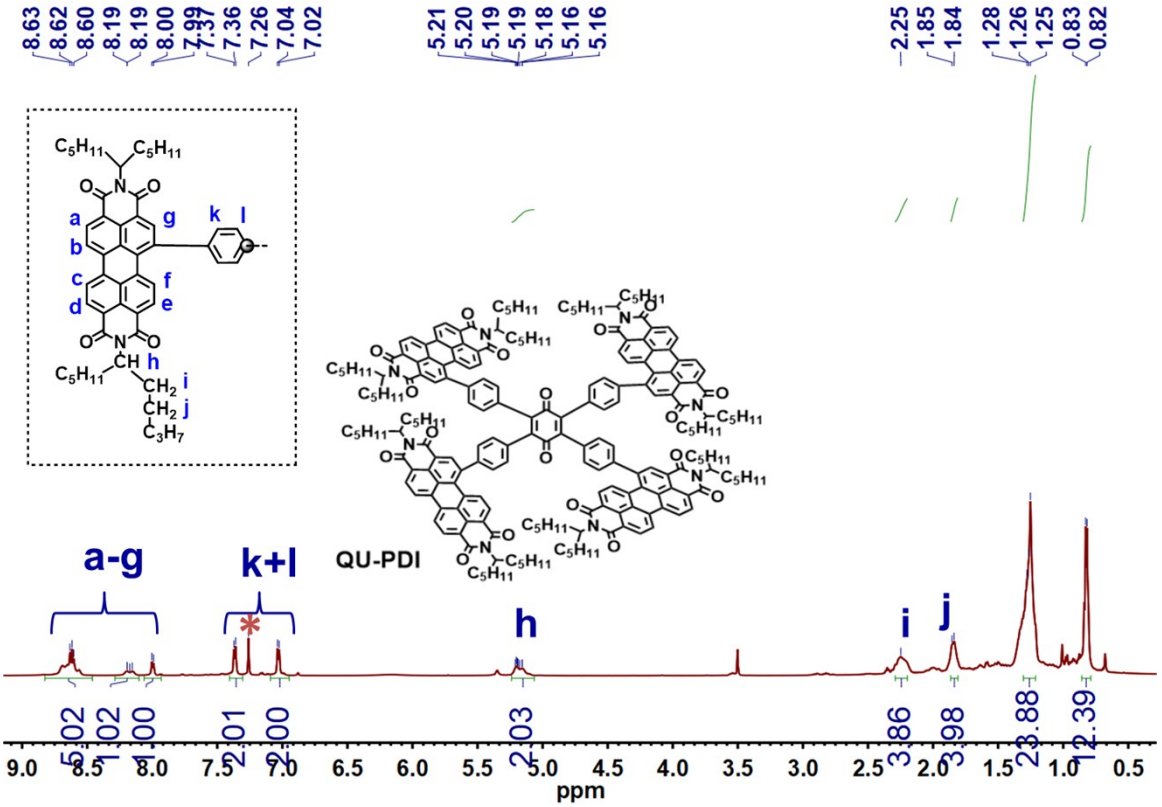

Figure S14. ^{1}H NMR spectrum of compound **QU-PDI**.

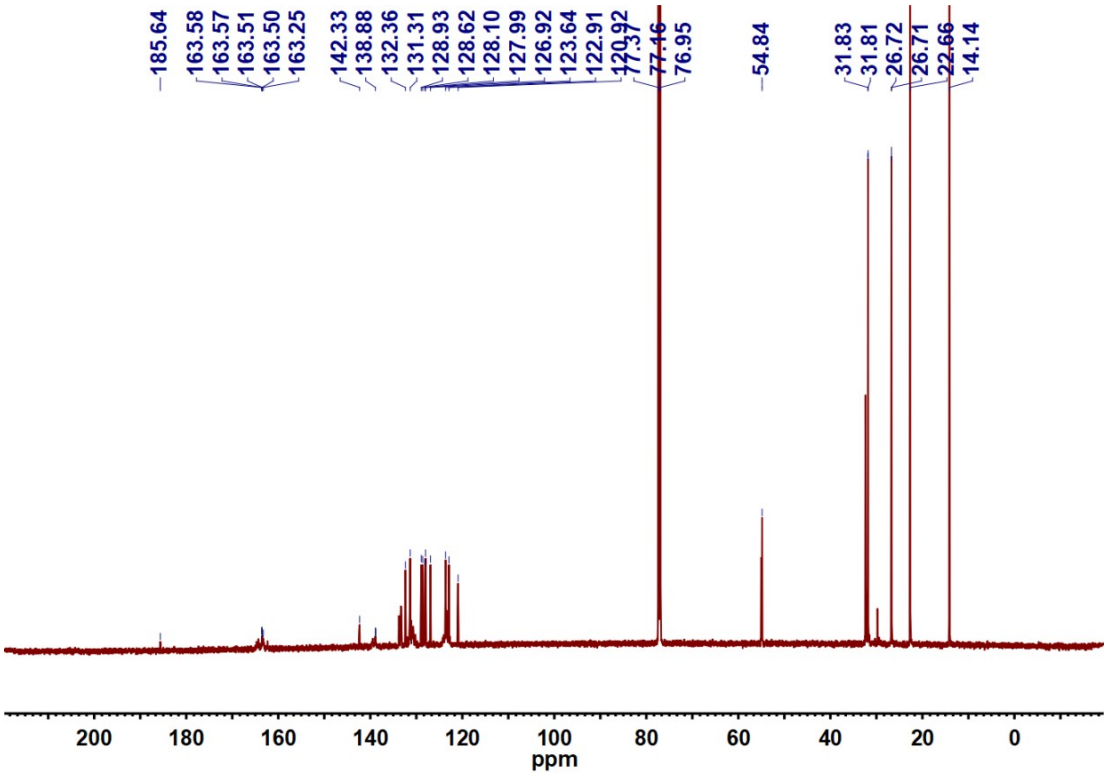

Figure S15. ^{13}C NMR spectrum of compound **QU-PDI**.

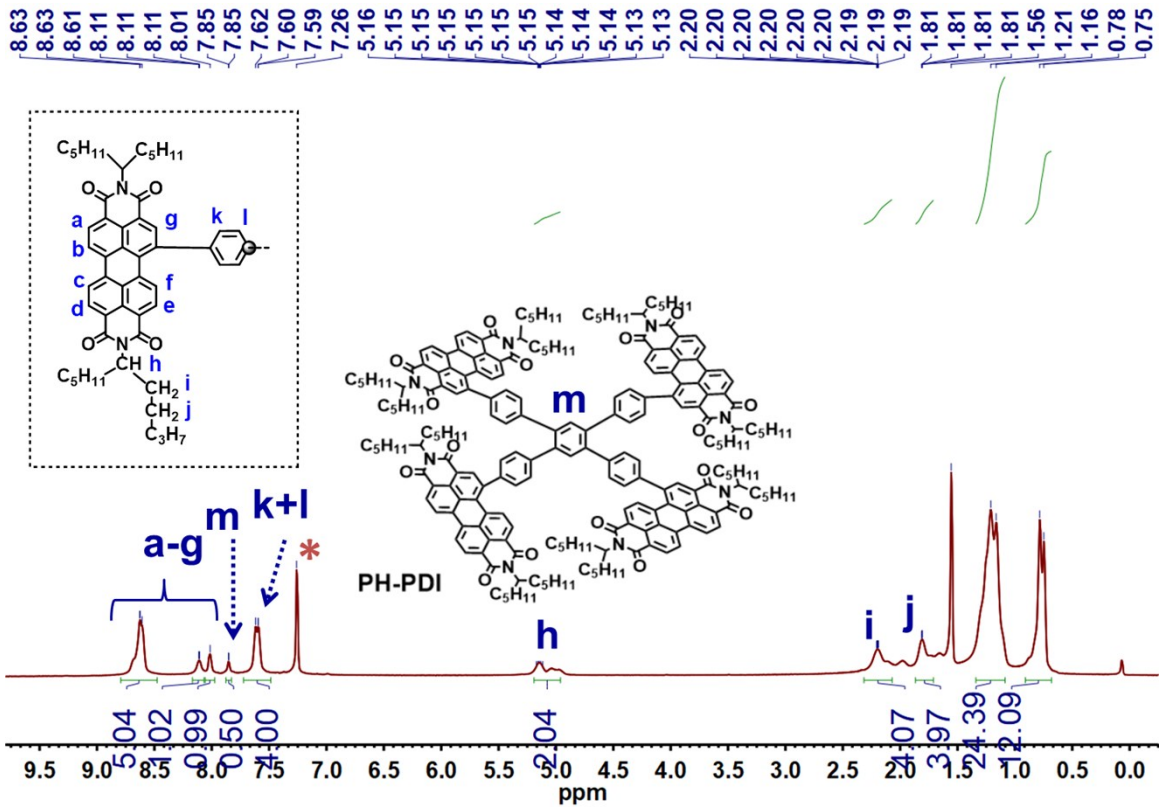

Figure S16. ^{1}H NMR spectrum of compound **PH-PDI**

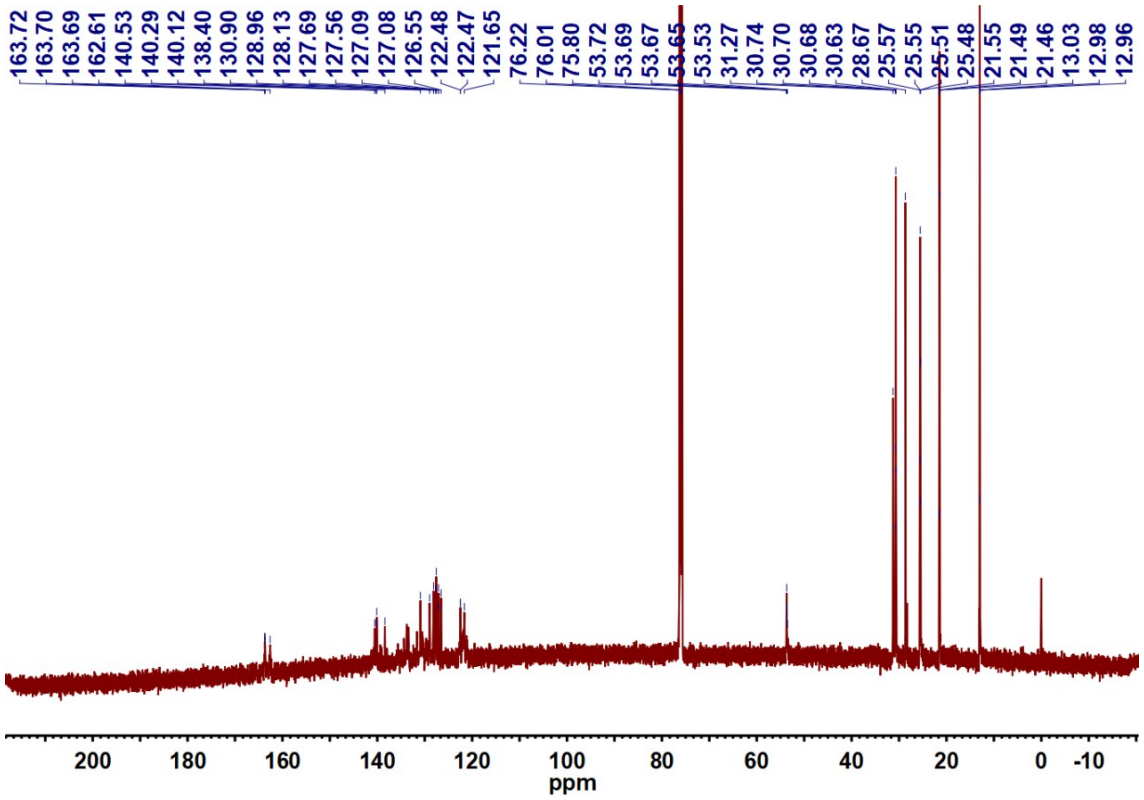

Figure S17. ^{13}C NMR spectrum of compound **PH-PDI.**

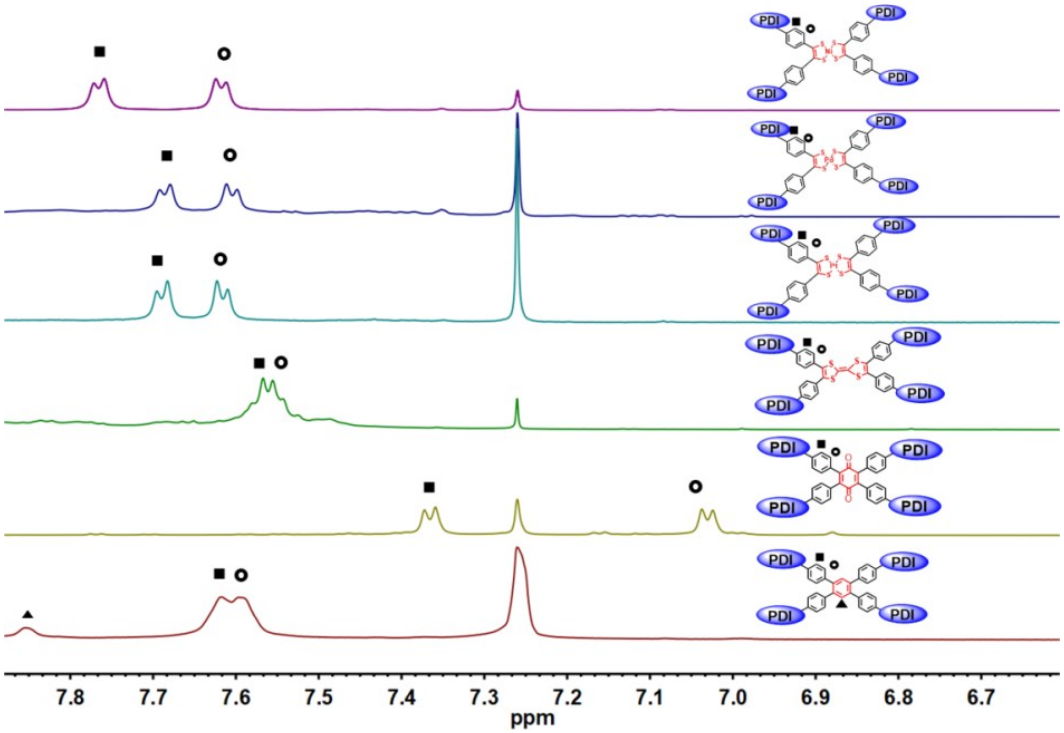

Figure S18. Comparisons of ^{1}H NMR spectra of six PDI propellers.

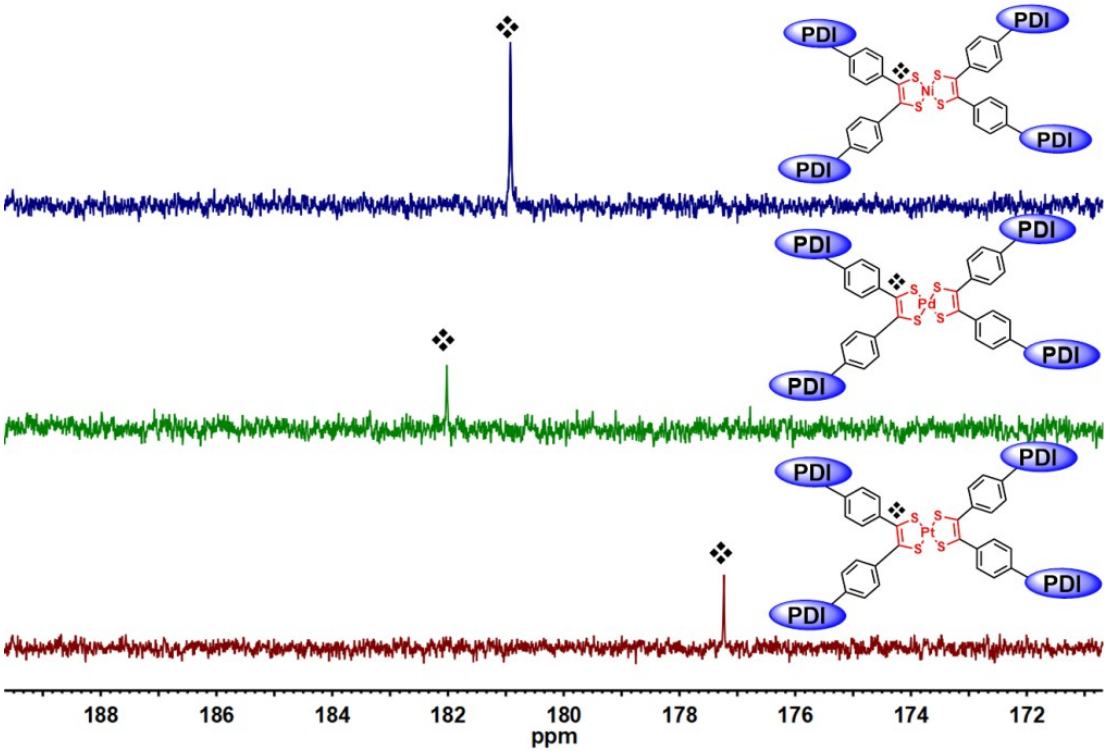

Figure S19. Comparisons of ^{13}C NMR spectra of PDI propellers with d^{8} metal cores.

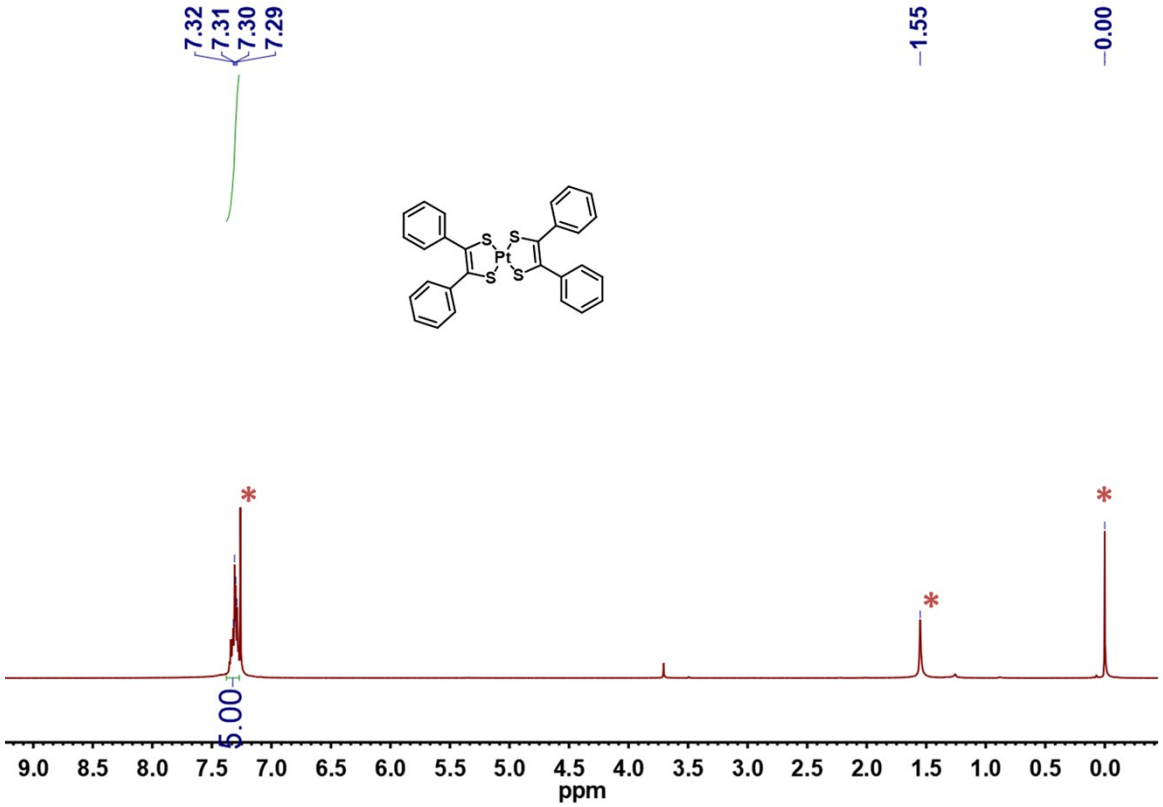

Figure S20. ^{1}H NMR spectrum of compound **Pt-PH.**

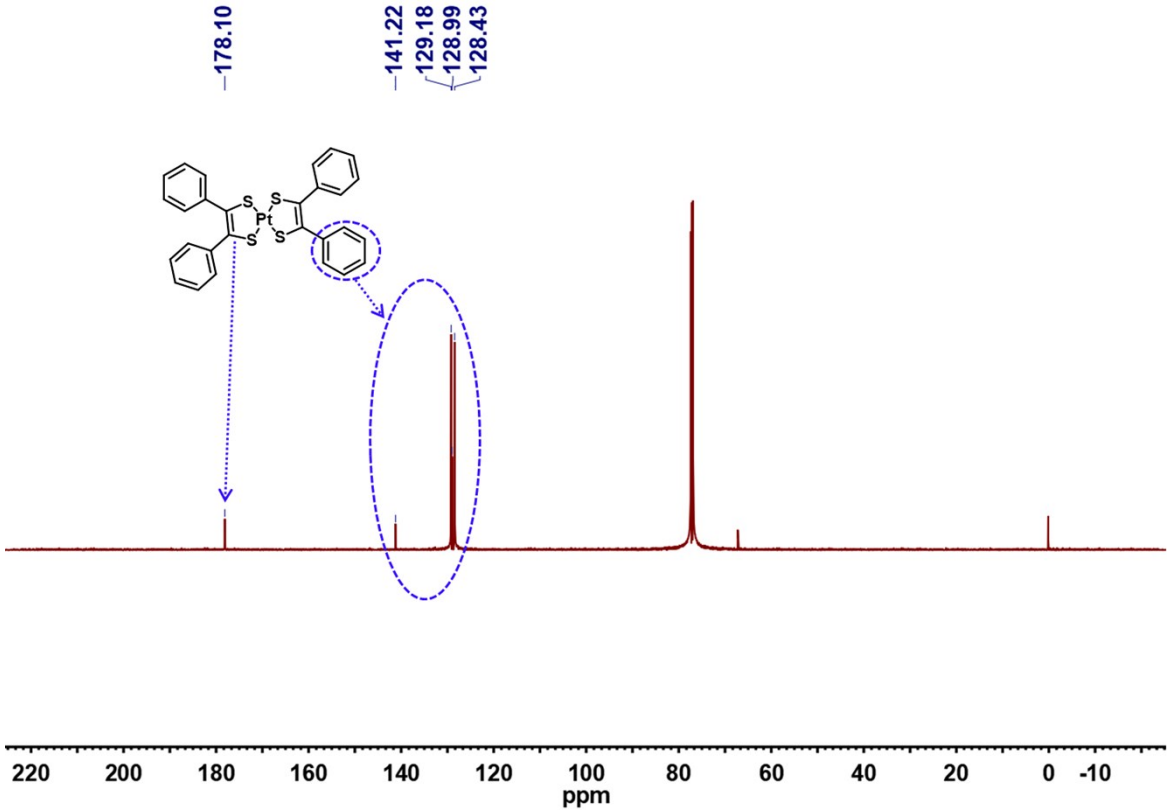

Figure S21. ^{13}C NMR spectrum of compound **Pt-PH.**

4. Mass Spectra of Compounds

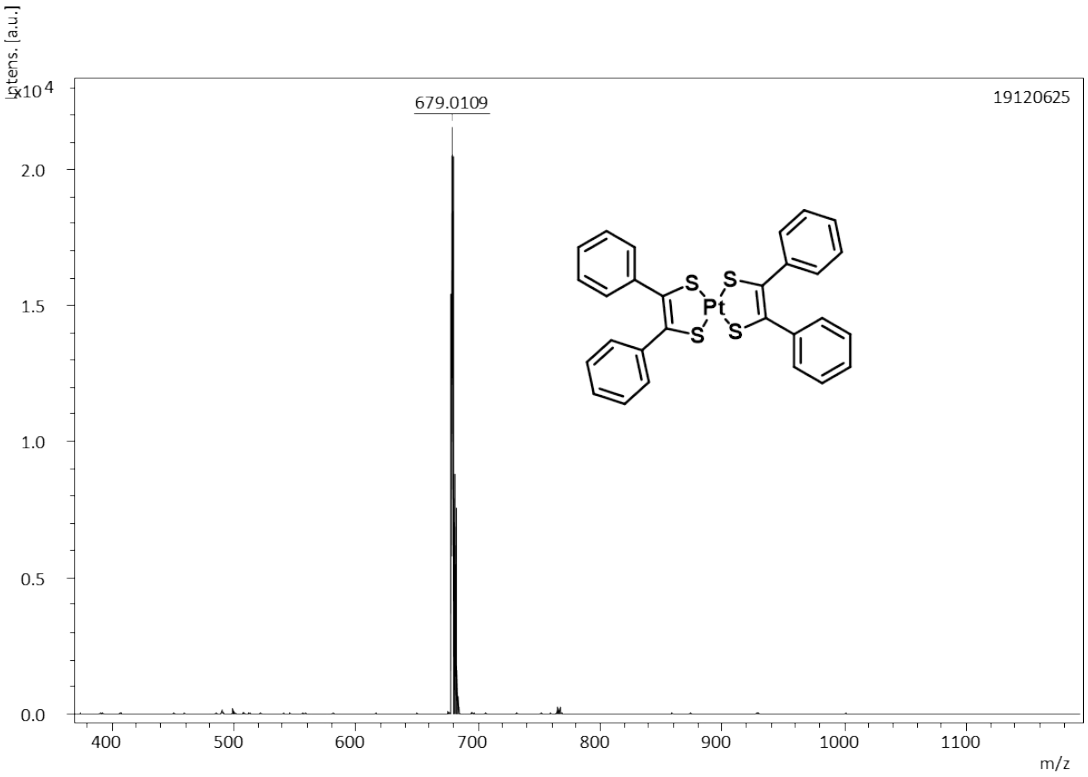

Figure S22. HRMS of **Pt-PH.**

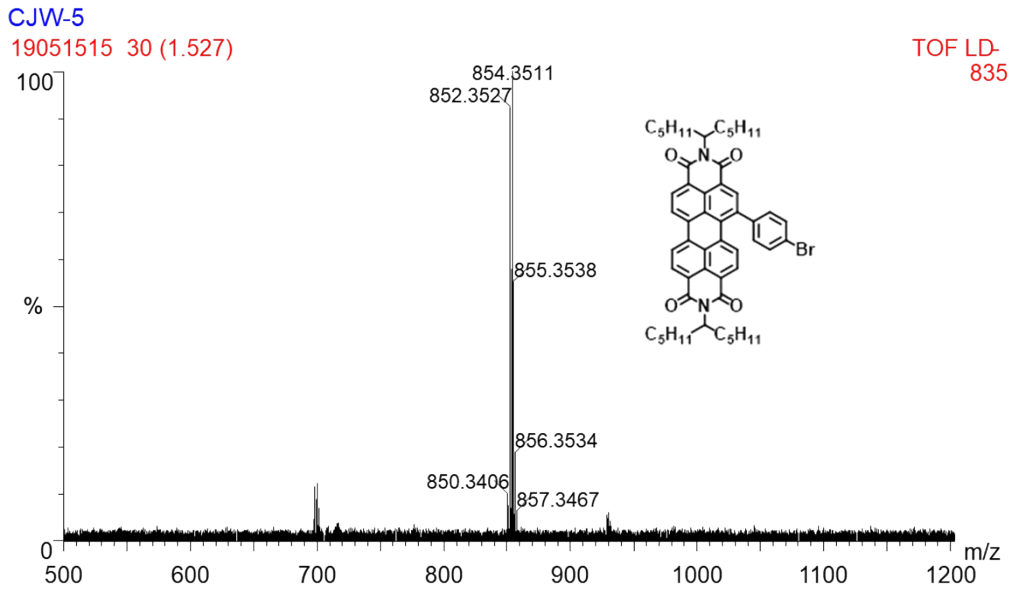

Figure S23. HRMS of compound **5.**

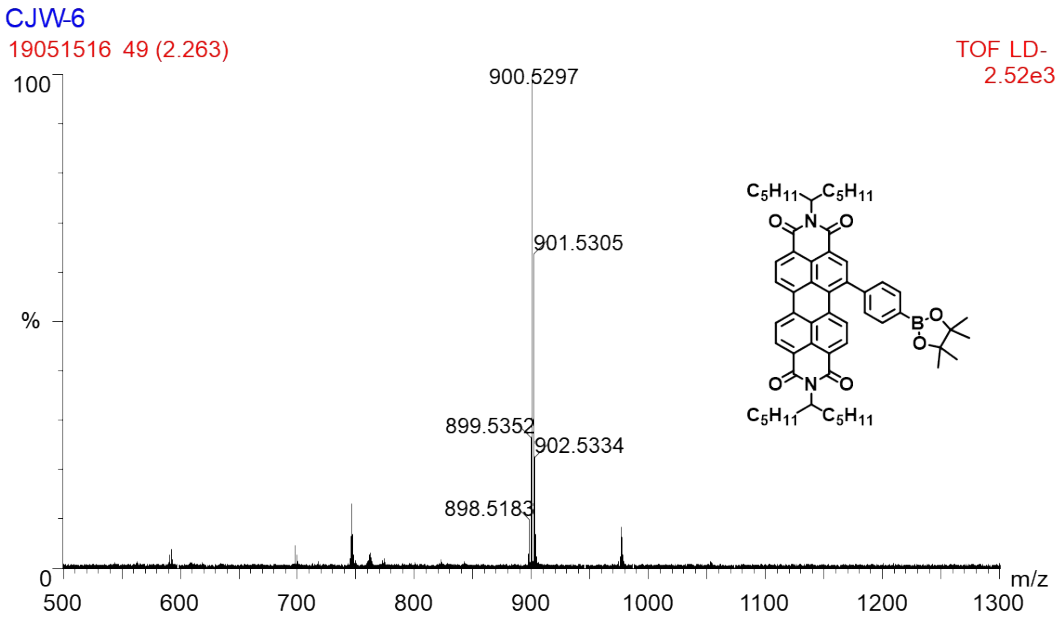

Figure S24. HRMS of compound **7.**

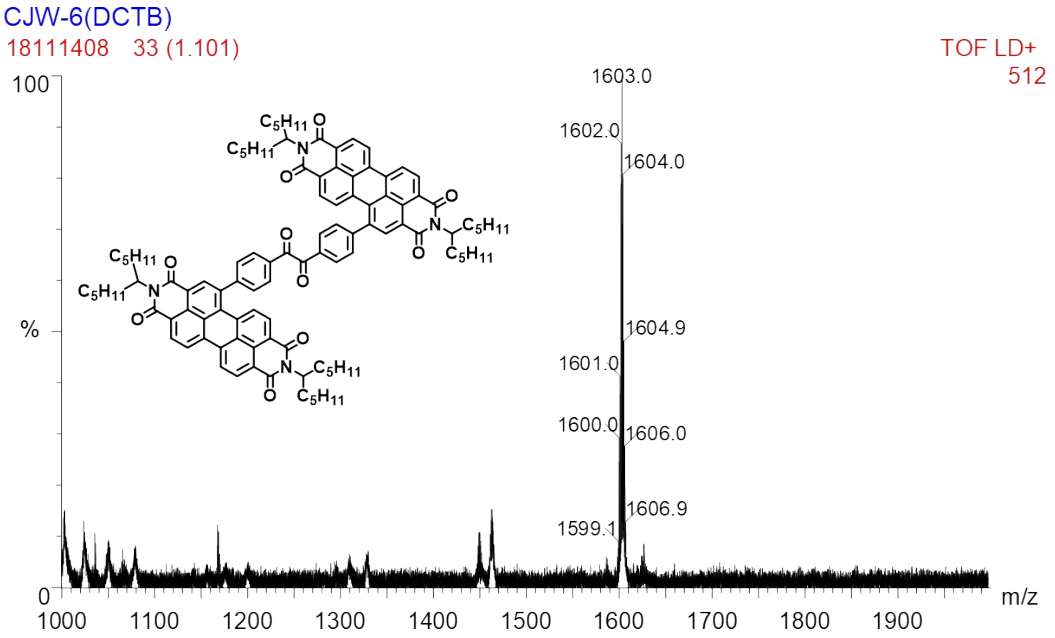

Figure S25. MALDI-TOF-MS of compound **3**.

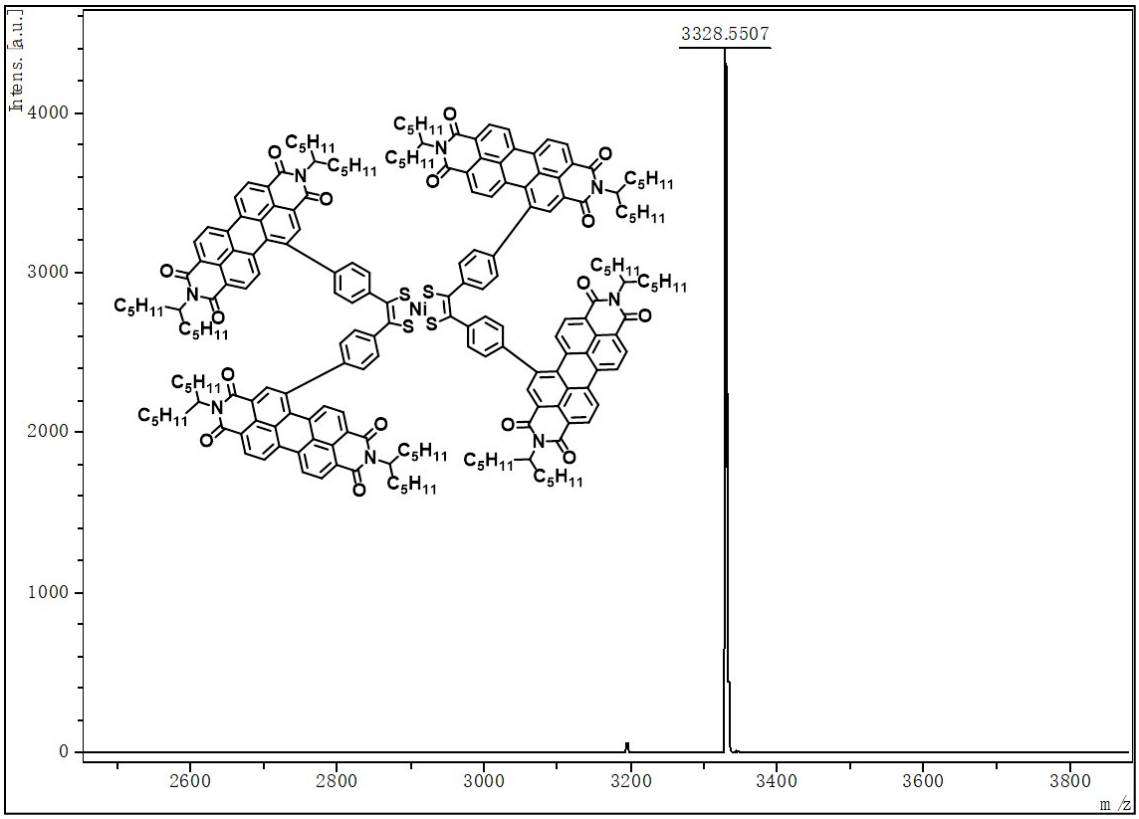

Figure S26. HRMS of **Ni-PDI.**

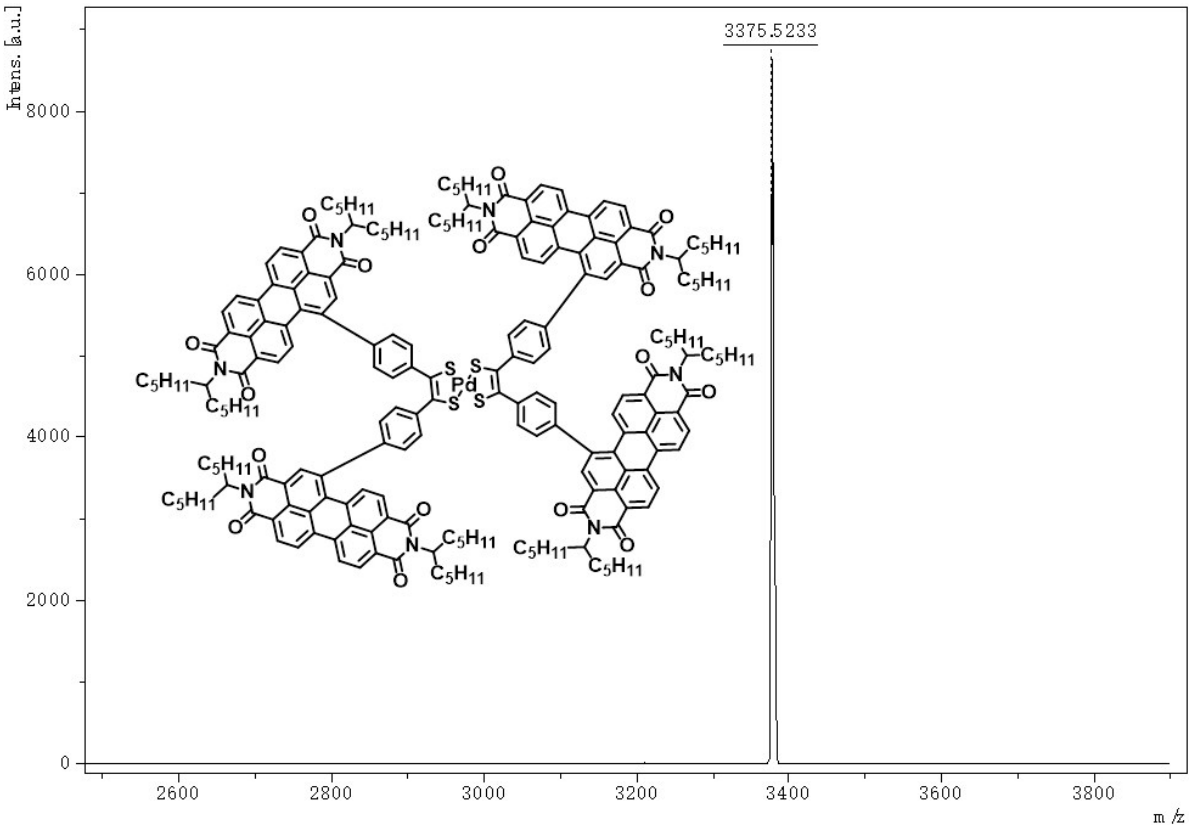

Figure S27. HRMS of **Pd-PDI**.

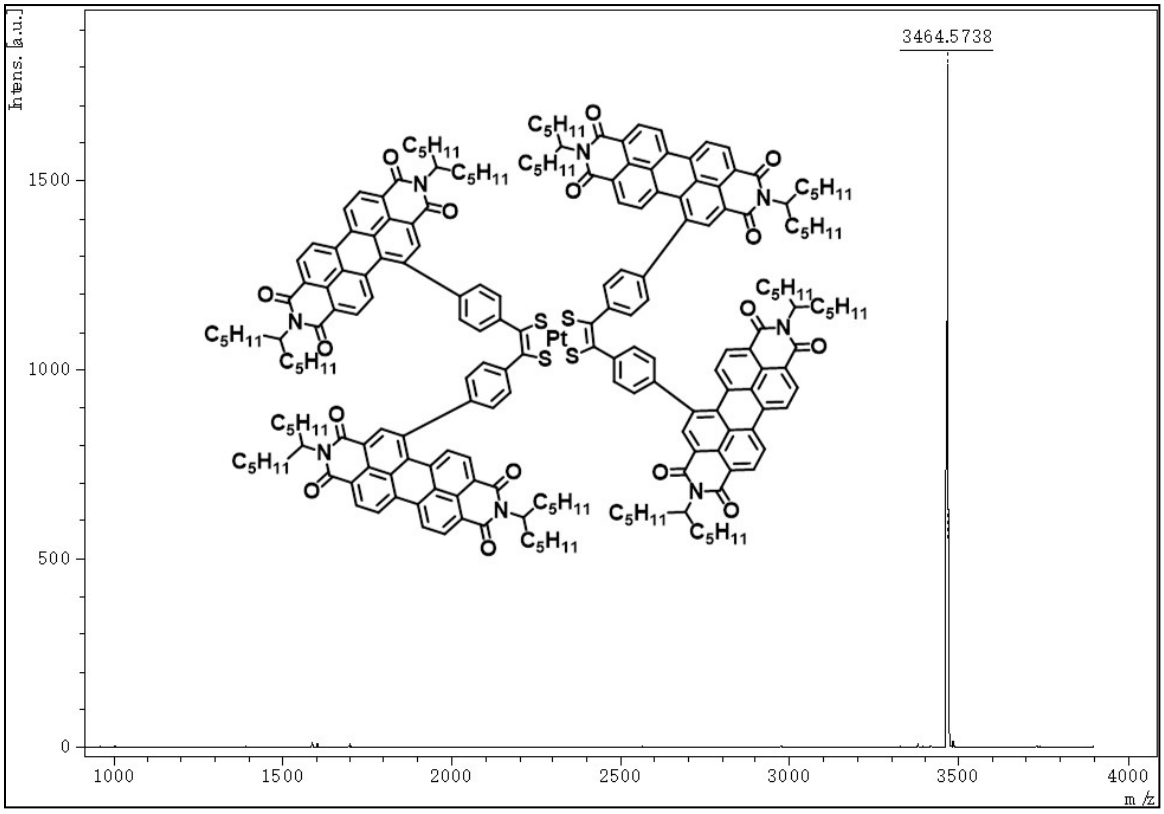

Figure S28. HRMS of **Pt-PDI**.

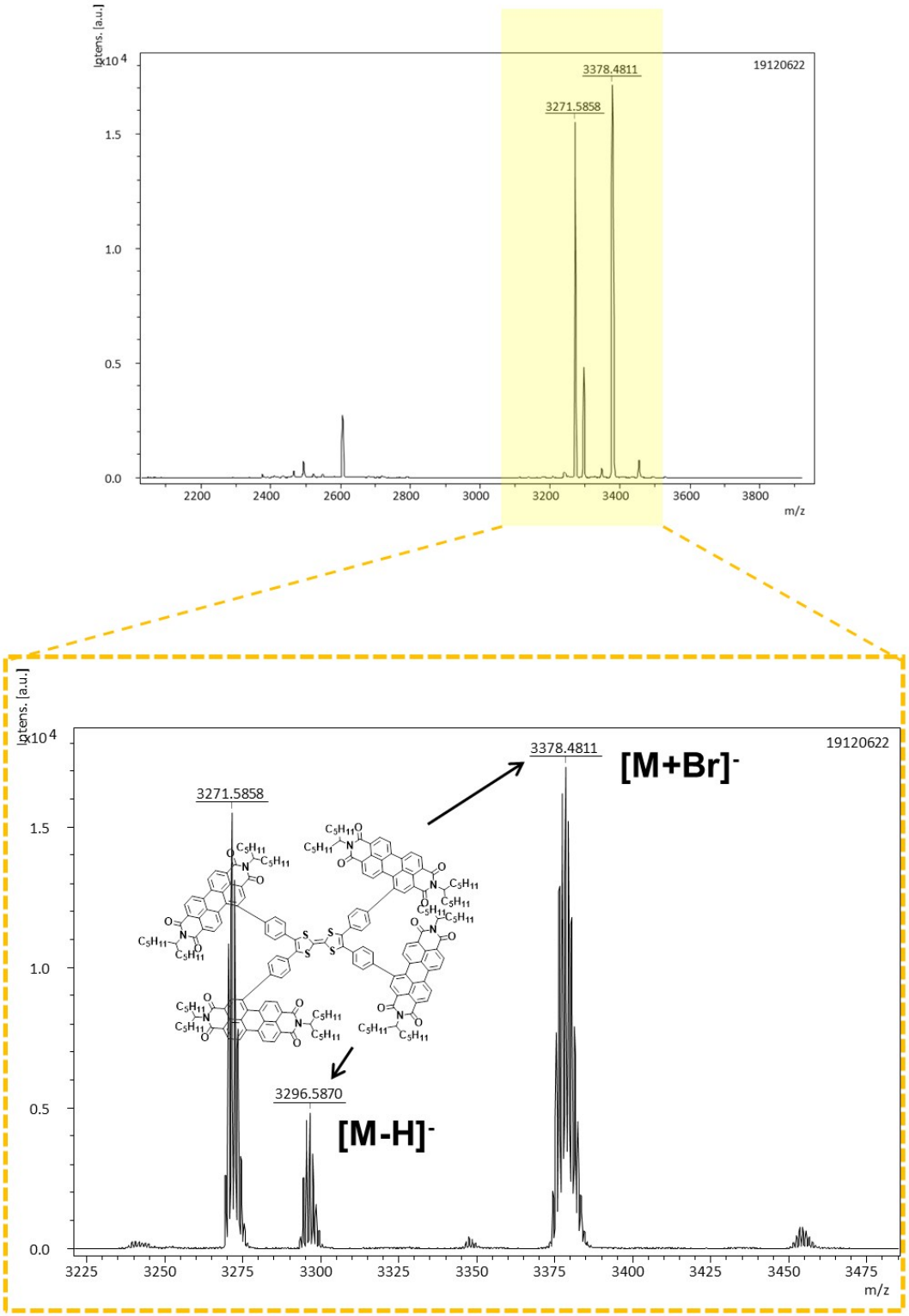

Figure S29. HRMS of **TTF-PDI.**

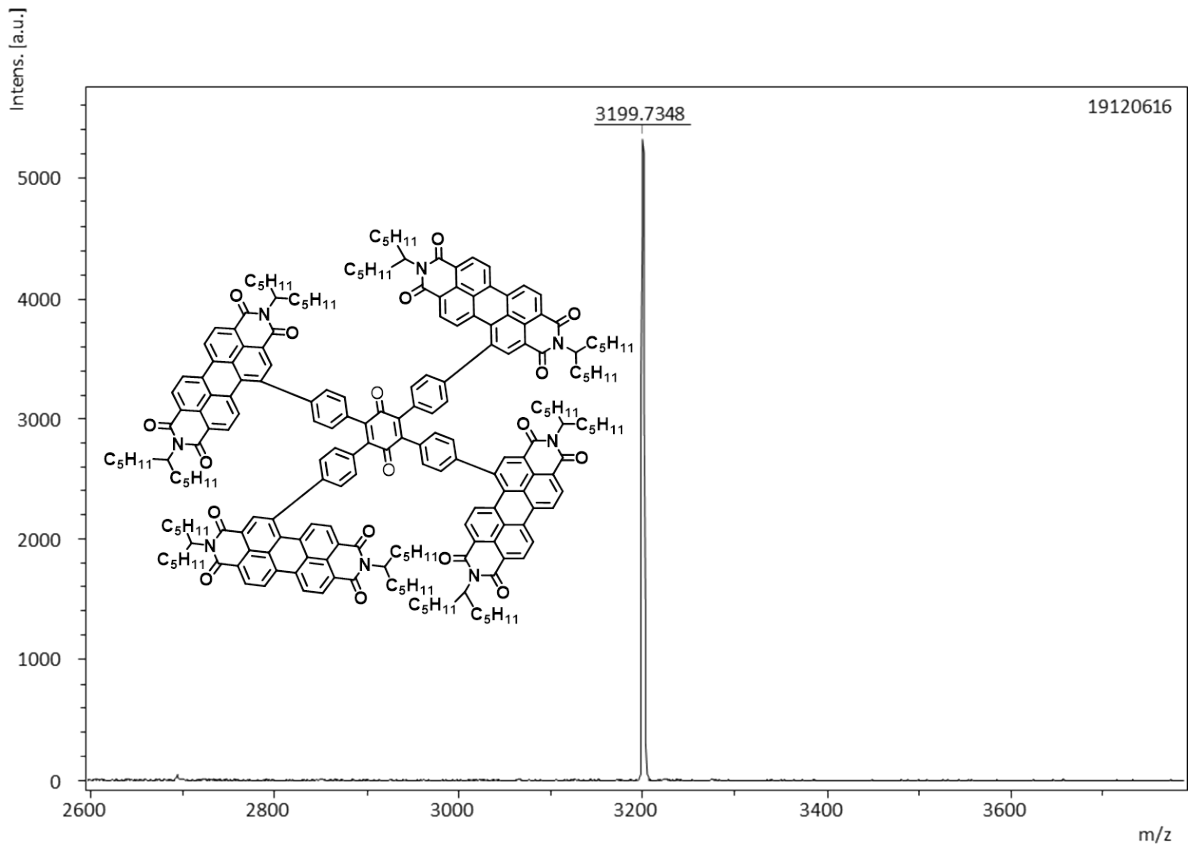

Figure S30. HRMS of **QU-PDI.**

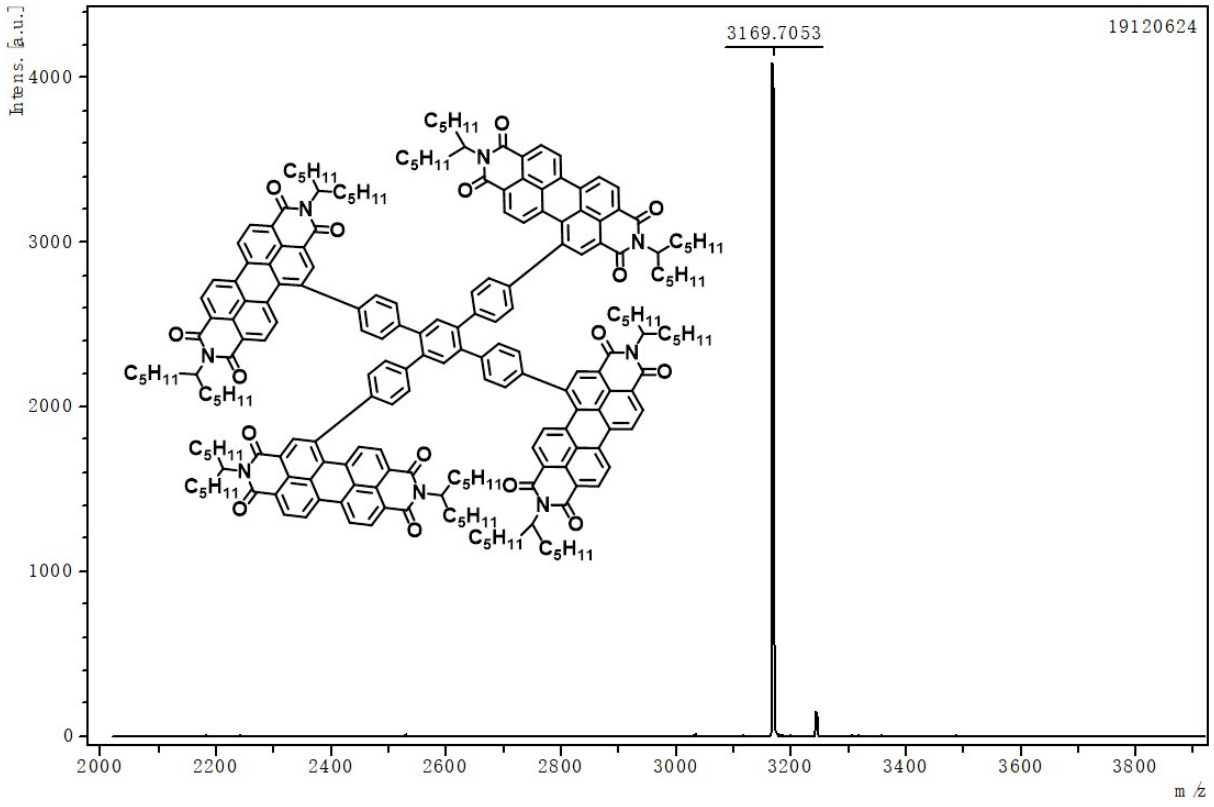

Figure S31. HRMS of **PH-PDI.**

5. Byproduct Analysis in the Synthesis of PDI Propeller Complexes

In our work, yields of PDI propeller complexes are quiet low at 9-23%. When 1.2-2.0 equiv. of P_4S_{10} (to benzil group) was used, as recommended by literatures,[13-16] trace of PDI propeller complexes were observed with large amount of unreacted start materials. When we use large excess of P_4S_{10} (near 10.0 equiv.), PDI propeller complexes are obtained after column chromatography isolation and slow diffusion of MeOH on a solution of the product in CH_2Cl_2. The low yield obtained in the case of PDI propeller complexes may have been due to the steric hindrance effect and low reactiviy of such large size of PDI-type ligands. As shown in Figure S32, one of the carbonyl group in benzil group is reduced to methylene. Some unreacted start materials still exist as can been seen in Figure S32. The structure of byproduct is confirmed by ^{1}H-NMR, ^{13}C-NMR and HRMS in Figure S33-S35.

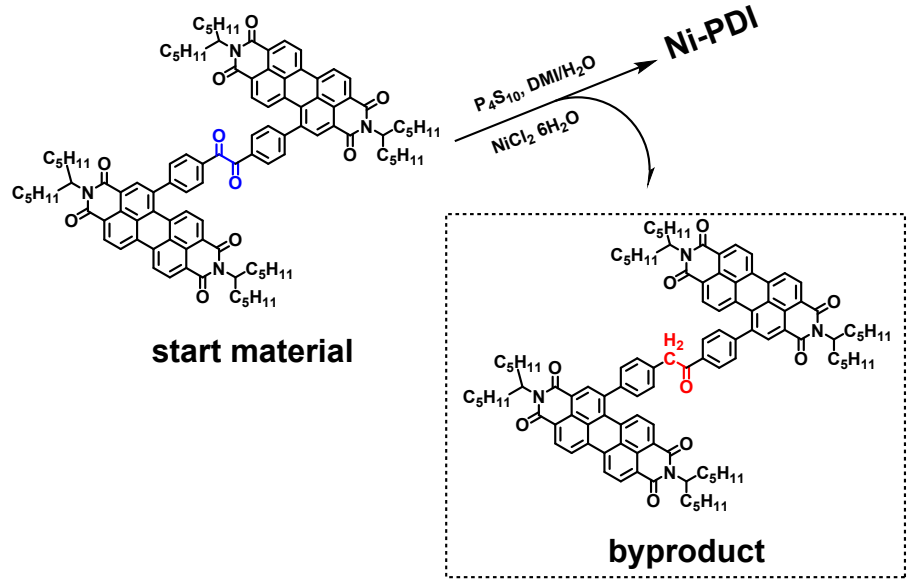

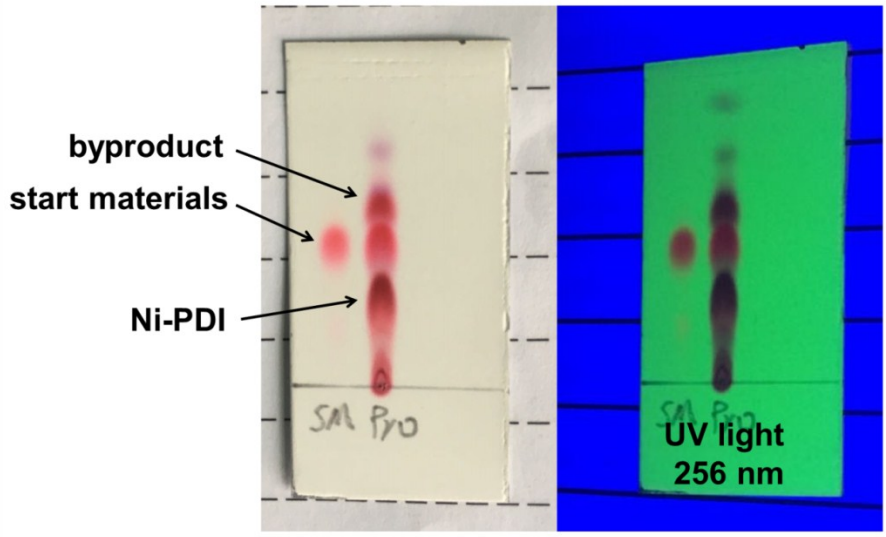

Figure S32. Byproduct analysis

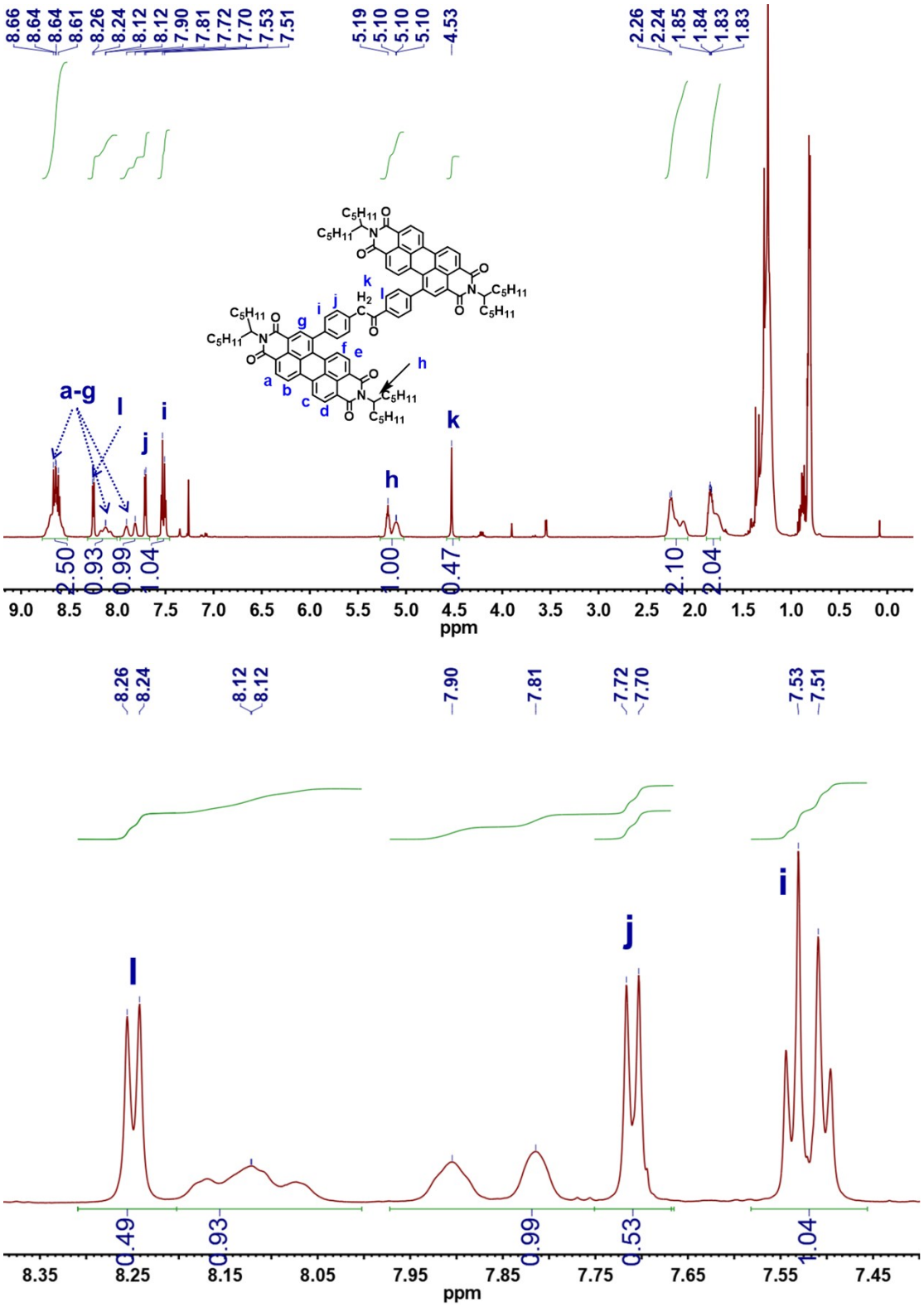

Figure S33. ^{1}H NMR spectrum of byproduct.

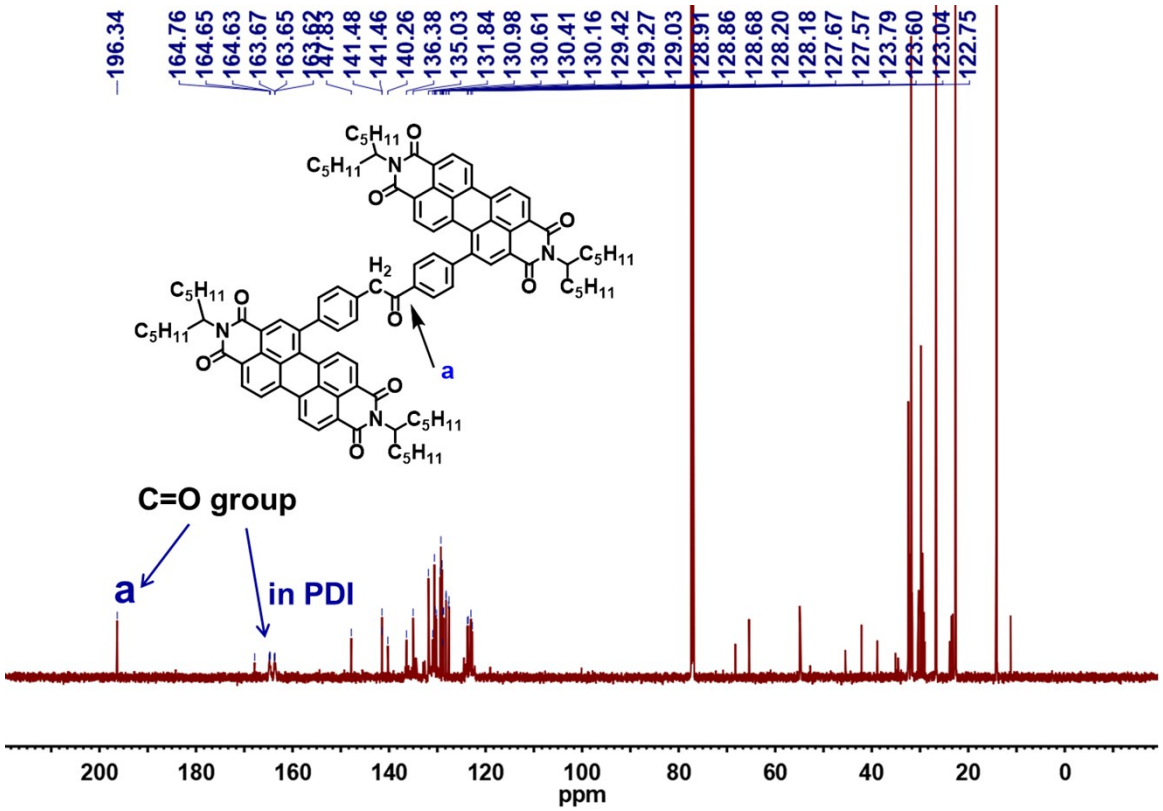

Figure S34. ^{13}C NMR spectrum of byproduct.

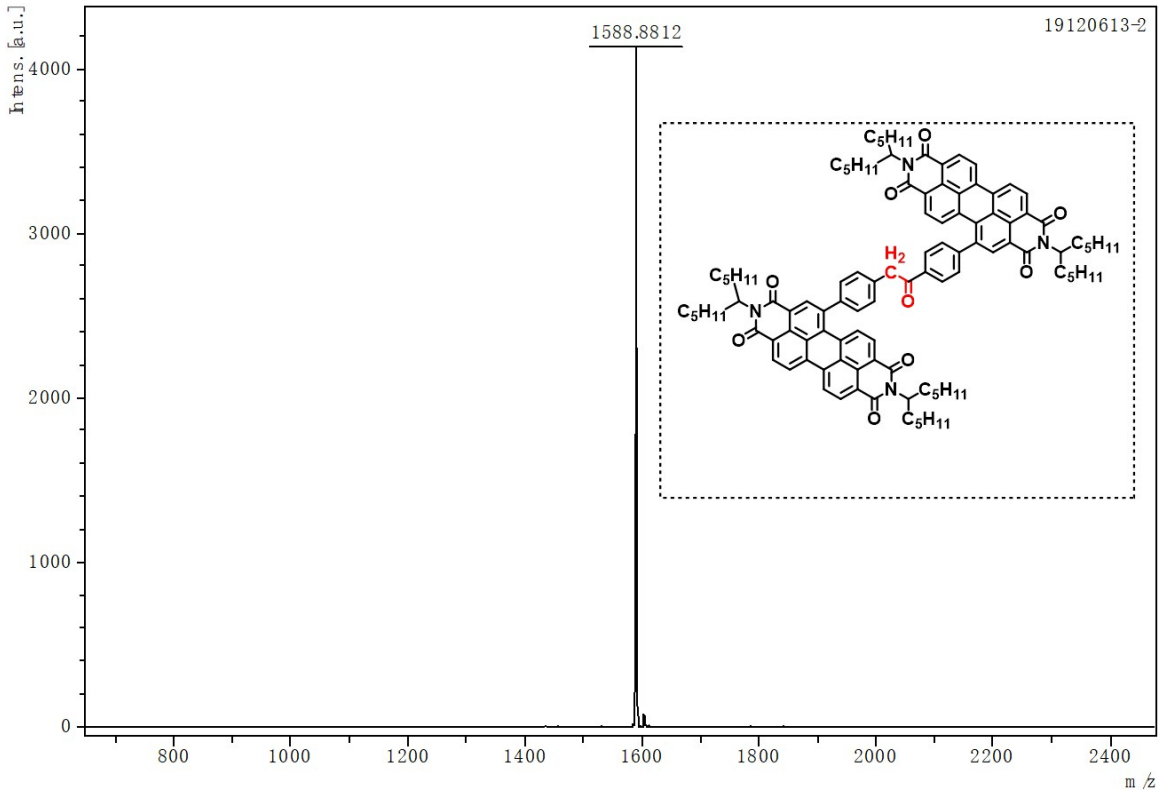

Figure S35. HRMS of byproduct.

6. Thermal Properties, Cyclic Voltammetries and UPS spectra

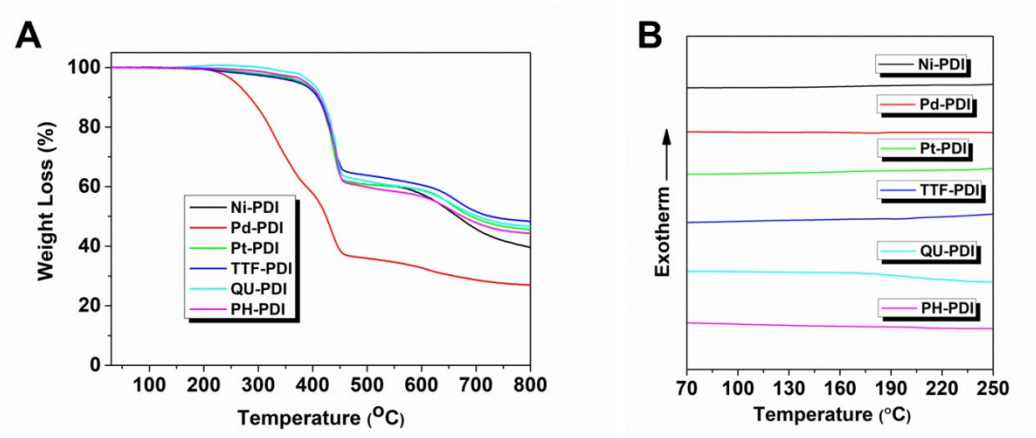

Figure S36. TGA and DSC curves of PDI propellers. The temperature of 5% thermal weight loss: Ni-PDI: $T_{d5\%}$=381 °C, Pd-PDI: $T_{d5\%}$=259 °C, Pt-PDI: $T_{d5\%}$=381 °C, TTF-PDI: $T_{d5\%}$= 372 °C, QU-PDI: $T_{d5\%}$=398 °C, PH-PDI: $T_{d5\%}$=389 °C.

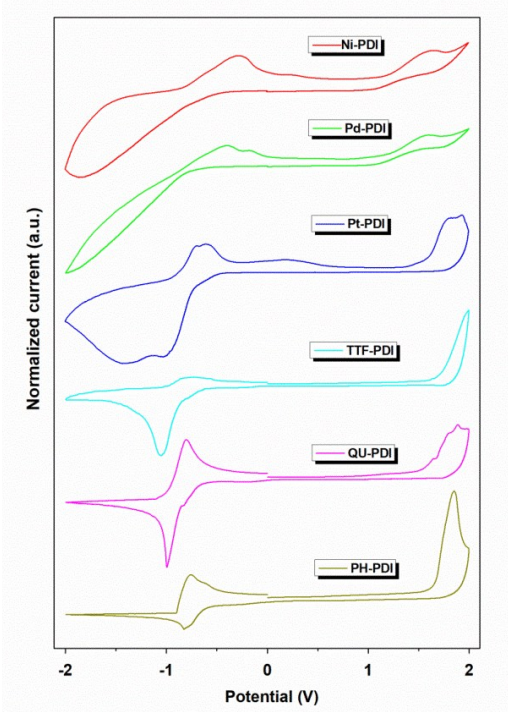

Figure S37. CV curves of PDI propellers (scan rate: 100 mV s^{-1}).

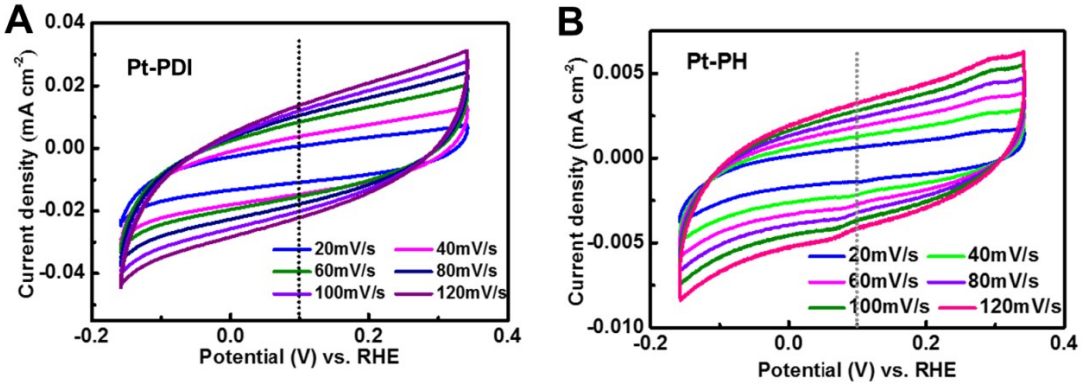

Figure S38. Pt-PDI and Pt-PH catalysts in 0.5 M H_2SO_4 with different scan rates of 20, 40, 60, 80, 100 and 120 mV s^{-1}.

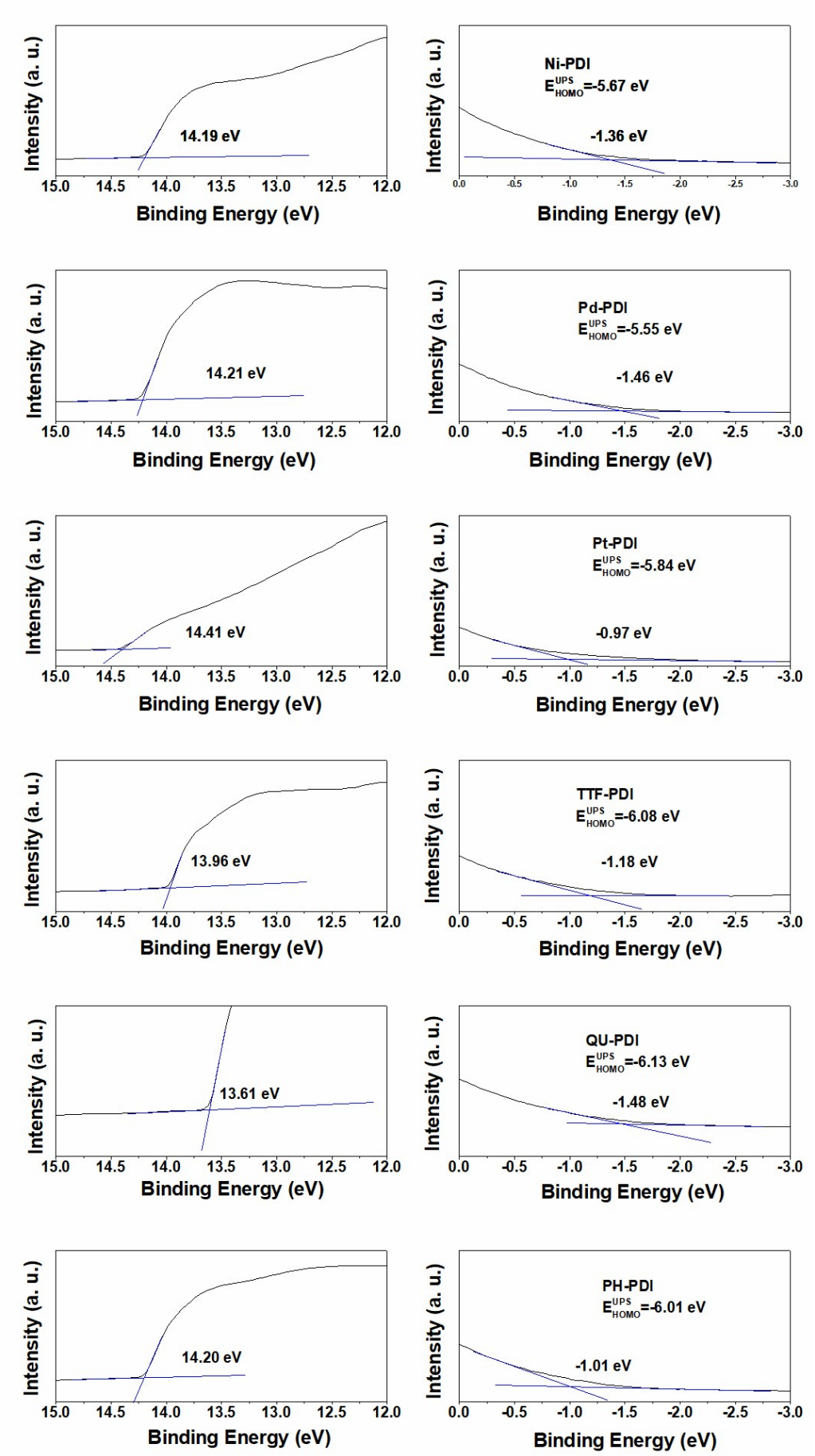

Figure S39. UPS spectra of PDI propellers.

7. Absorption and PL Spectra of the Molecules

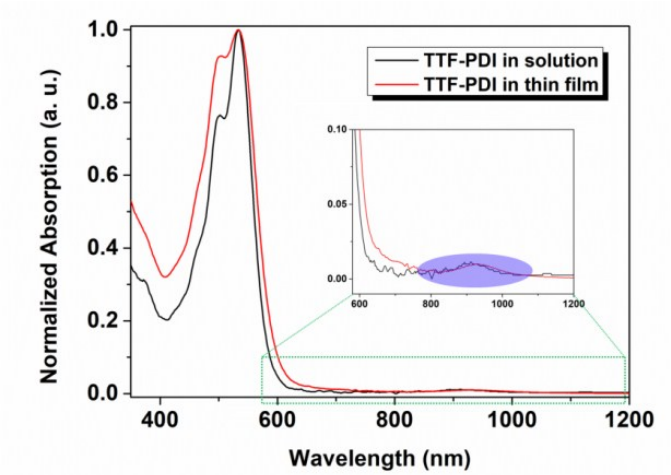

Figure S40. UV-vis spectra of TTF-PDI, the blade PDI and core TTF charge transfer complex peak around 912 nm.

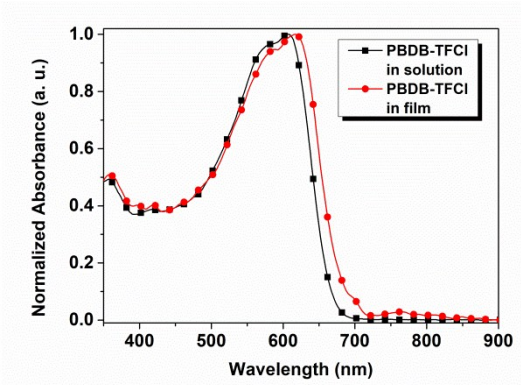

Figure S41. UV-vis spectra of polymer donor PBDB-TFCl.

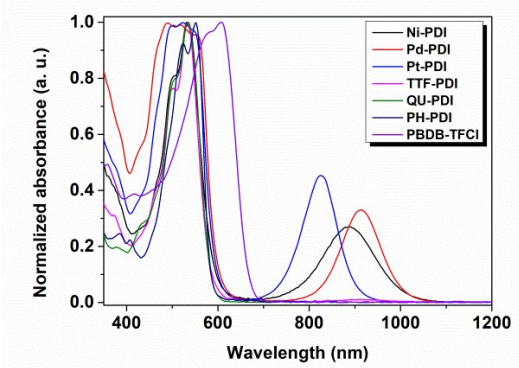

Figure S42. UV-vis spectra of polymer donor PBDB-TFCl and PDI propellers in chloroform solution.

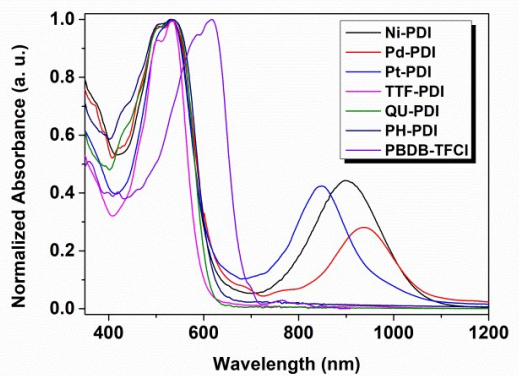

Figure S43. UV-vis spectra of polymer donor PBDB-TFCl and PDI propellers in thin film.

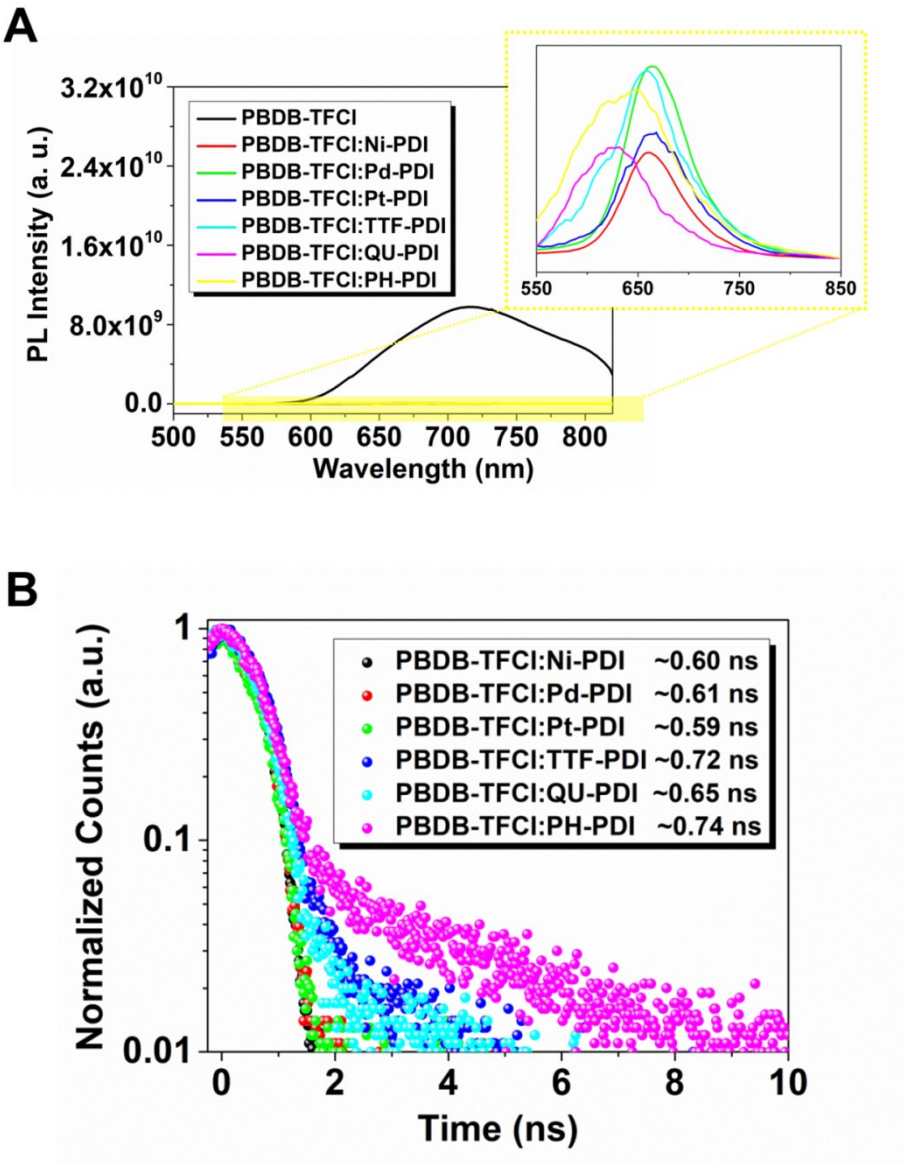

Figure S44. Steady-state photoluminescence measurements for (A) PBDB-TFCl:PDI propellers blend films and (B) Transient photoluminescence of PBDB-TFCl:PDI propellers blend films in response to 450 nm pulses (excited at 450 nm and monitored at 660 nm).

8. SCLC Mobilities, P(E,T), the J_{ph} versus V_{eff}, the V_{oc} and J_{sc} versus Light Intensity

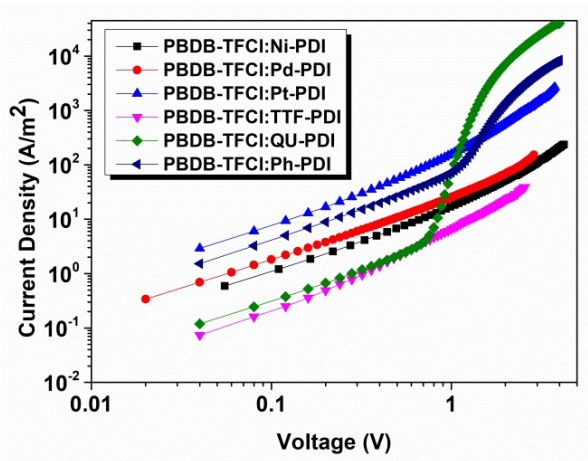

Figure S45. The electron mobility of polymer:PDI propeller fabricated blends under optimized conditions based on SCLC measurements.

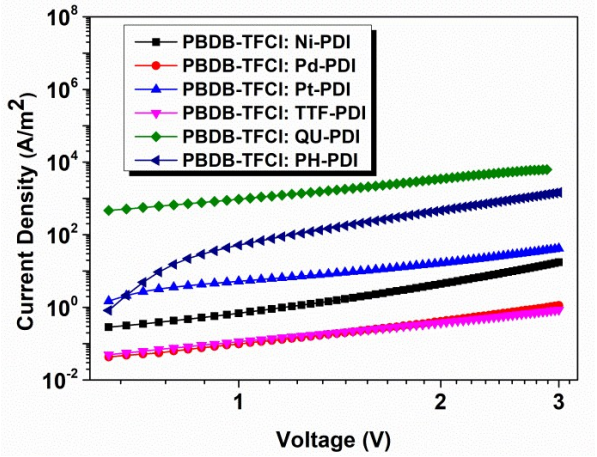

Figure S46. The hole mobility of polymer:PDI propeller fabricated blends under optimized conditions based on SCLC measurements.

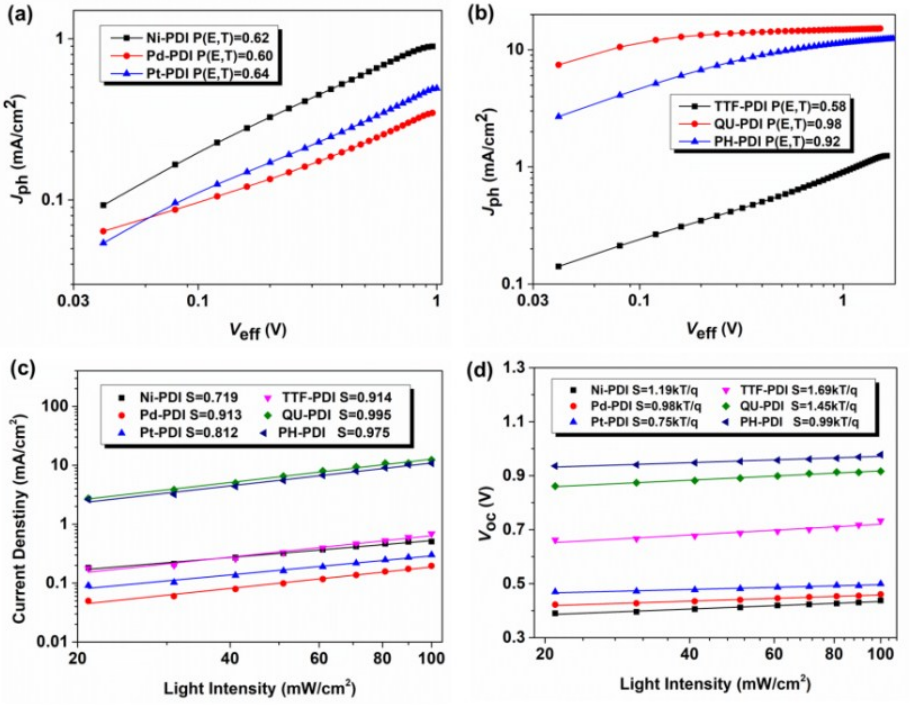

Figure S47. (a, b) The J_{ph} versus V_{eff}, (c) the J_{sc} versus light intensity and (d) the V_{oc} versus light intensity for the optimized d^8 metal and non-metal cores PDI propeller-based OPV decives.

9. Photovoltaic Device Fabrication and Characterization

Table S1. Photovoltaic Parameters of the Optimized PBDB-TFCl:Ni-PDI Propeller Acceptor Solar Cells under AM 1.5G Illumination of 100 mW/cm^2

Donor:Acceptor	Conditions[a]	V_{OC} (V)	J_{SC} (mA/cm^2)	FF (%)	PCE (%)[b]
PBDB-TFCl:Ni-PDI	1:1 Without DIO	0.45	0.39	33.6	0.060
	0.5% DIO	0.42	0.28	33.0	0.038
	1.0% DIO	**0.43**	**0.53**	**32.3**	**0.074**
	1.5% DIO	0.42	0.49	30.9	0.064
	TA[c]	0.44	0.46	33.9	0.069

[a]Herein, 1:1 stands for the mass ratio of donor:acceptor. DIO stands for the additive 1,8-diiodooctane. 0.5% stands for the volume ratio of DIO to chlorobenzene solvent. [b]The best PCE based on at least ten devices. [c]Thermal annealing (TA) at 110 ˚C for 10 min.

Table S2. Photovoltaic Parameters of the Optimized PBDB-TFCl:Pd-PDI Propeller Acceptor Solar Cells under AM 1.5G Illumination of 100 mW/cm^2

Donor:Acceptor	Conditions	V_{OC} (V)	J_{SC} (mA/cm^2)	FF (%)	PCE (%)[b]
PBDB-TFCl:Pd-PDI	**1:1 Without DIO**	**0.47**	**0.21**	**34.9**	**0.034**
	0.5% DIO	0.38	0.16	28.1	0.017
	1.0% DIO	0.30	0.16	27.1	0.013
	1.5% DIO	0.47	0.20	29.9	0.028
	TA[a]	0.45	0.21	35.9	0.034

[a]Thermal annealing (TA) at 110 ˚C for 10 min. [b]The best PCE based on at least ten devices.

Table S3. Photovoltaic Parameters of the Optimized PBDB-TFCl:Pt-PDI Propeller Acceptor Solar Cells under AM 1.5G Illumination of 100 mW/cm^2

Donor:Acceptor	Conditions	V_{OC} (V)	J_{SC} (mA/cm^2)	FF (%)	PCE (%)[b]
PBDB-TFCl:Pt-PDI	**1:1 Without DIO**	**0.51**	**0.33**	**34.2**	**0.057**
	0.5% DIO	0.45	0.18	33.7	0.027
	1.0% DIO	0.42	0.19	29.7	0.024
	1.5% DIO	0.45	0.18	33.6	0.027
	TA[a]	0.49	0.31	34.9	0.053

[a]Thermal annealing (TA) at 110 ˚C for 10 min. [b]The best PCE based on at least ten devices.

Table S4. Photovoltaic Parameters of the Optimized PBDB-TFCl:TTF-PDI Propeller Acceptor Solar Cells under AM 1.5G Illumination of 100 mW/cm^2

Donor:Acceptor	Conditions	V_{OC} (V)	J_{SC} (mA/cm^2)	FF (%)	PCE (%)[b]
PBDB-TFCl:TTF-PDI	1:1 Without DIO	0.71	0.41	37.1	0.109
	0.5% DIO	0.69	0.47	36.1	0.119
	1.0% DIO	**0.73**	**0.69**	**35.3**	**0.178**
	1.5% DIO	0.63	0.61	36.9	0.143
	1.0% DIO+ TA[a]	0.68	0.58	38.6	0.153
	TA	0.68	0.41	37.7	0.104

[a]Thermal annealing (TA) at 110 ˚C for 10 min. [b]The best PCE based on at least ten devices.

Table S5. Photovoltaic Parameters of the Optimized PBDB-TFCl:QU-PDI Propeller Acceptor Solar Cells under AM 1.5G Illumination of 100 mW/cm^2

Donor:Acceptor	Conditions	V_{OC} (V)	J_{SC} (mA/cm^2)	FF(%)	PCE (%)[b]
PTBTz-2[17]:QU-PDI	1:1	0.89	3.35	53.5	1.60
PTBD-BDD[18]:QU-PDI	1:1	1.00	7.98	51.1	4.09
PBDB-TFCl[19]:QU-PDI	1:1	0.96	11.33	52.6	5.73
	1:1 with 0.25% DIO	0.93	14.10	58.4	7.66
	1:1 with 0.5% DIO	0.91	14.53	64.7	8.58
	1:1 with 1.0% DIO	**0.93**	**14.02**	**71.8**	**9.33**
	1:1 with 1.5% DIO	0.91	13.16	71.1	8.49
	1:1 with 1.0% DIO+TA[a]	0.91	13.50	70.9	8.76
	1:1.5 with 1.0%DIO	0.89	13.69	66.2	8.09
	1.5:1 with 1.0%DIO	0.87	10.70	58.6	5.44

[a]Thermal annealing (TA) at 110 ˚C for 10 min. [b]The best PCE based on at least ten devices.

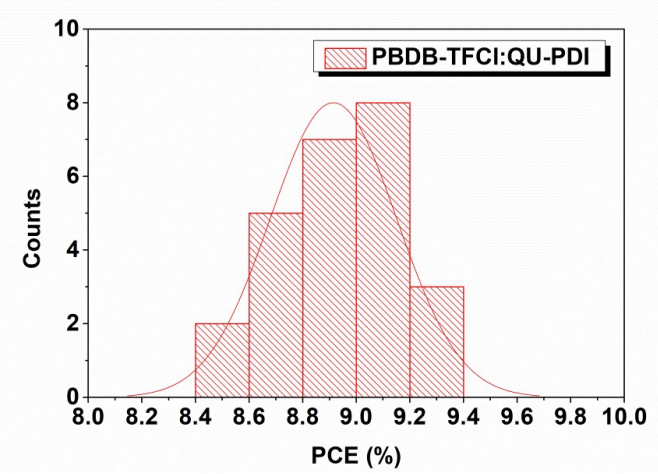

Figure S48. Statistical PCE distribution histograms of 25 PBDB-TFCl:QU-PDI solar cells.

Table S6. Photovoltaic Parameters of the Optimized PBDB-TFCl:PH-PDI Propeller Acceptor Solar Cells under AM 1.5G Illumination of 100 mW/cm^2

Donor:Acceptor	Conditions	V_{OC} (V)	J_{SC} (mA/cm^2)	FF (%)	PCE (%)[b]
PBDB-TFCl:PH-PDI	1:1	0.99	9.61	39.6	3.78
	1:1+TA[a]	0.98	10.00	41.3	4.06
	1:1 with 0.5% DIO	0.97	10.92	47.0	4.99
	1:1 with 1.0% DIO	0.97	11.98	49.0	5.68
	1:1 with 1.5% DIO	0.98	9.67	51.7	4.90
	1:1 with 1.0% DIO+TA	**0.95**	**11.66**	**54.4**	**6.01**

[a]Thermal annealing (TA) at 110 ˚C for 10 min. [b]The best PCE based on at least ten devices.

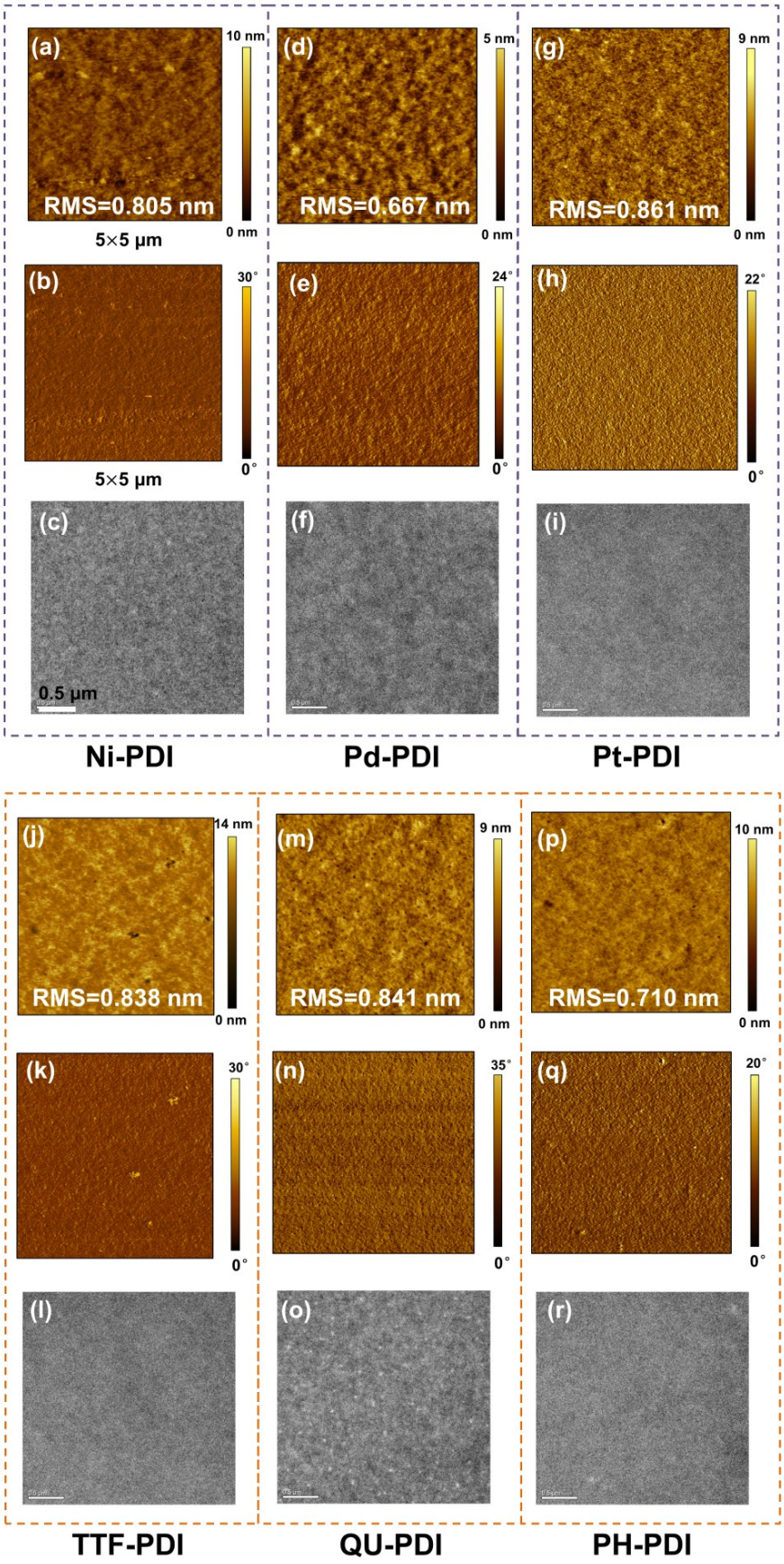

Figure S49. Morphology images of the blend films: (a,d,g,j,m,p) the AFM height, (b,e,h,k,n,q) AFM phase, and (c,f,i,l,o,r) TEM images of the PBDB-TFCl:PDI propellers blend films.

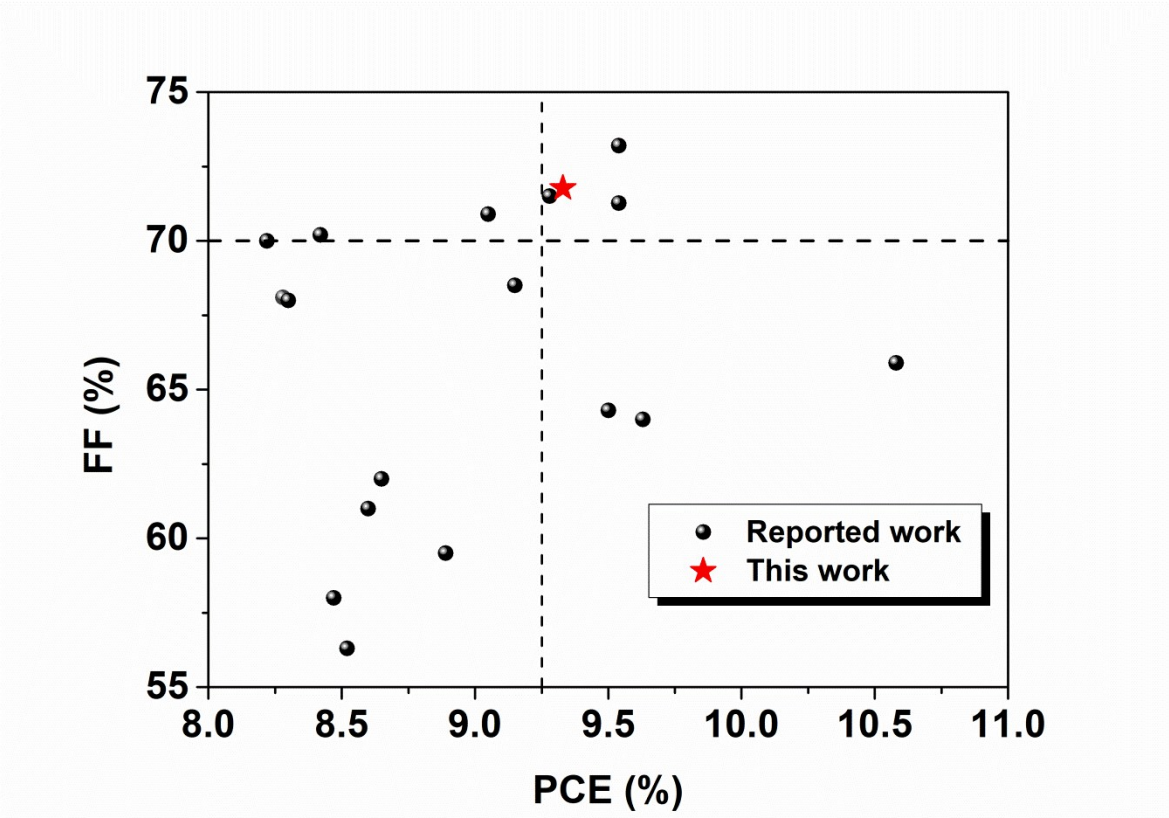

Figure S50. Plots of FF versus PCE for OPVs based on PDI-based acceptor with PCEs > 8%.

Table S7. Photovoltaic Parameters of OPVs Based on PDI-based Acceptor with PCEs > 8%

Acceptor	Donor	PCE (%)	FF	V_{oc} (V)	J_{sc} (mA/cm^2)	Ref.
QU-PDI	**PBDB-TFCl**	**9.33**	**0.718**	**0.93**	**14.02**	**this work**
SdiPBI-S	PBDTS-Se	8.22	0.70	0.91	12.9	Adv. Sci. 2016, 3, 1600117.
BPT-S	PDBT-T1	8.28	0.681	1.02	11.94	J. Mater. Chem. C 2018, 6, 1136-1142.
hPDI4	PTB7-Th	8.3	0.68	0.8	15.2	Nat. Commun.2015, 6:8242.
SdiPBI-Se	PDBT-T1	8.42	0.702	0.96	12.49	J. Am. Chem. Soc. 2016, 138, 375-380.
TPB	PTB7-Th	8.47	0.58	0.8	18.25	J. Am. Chem. Soc. 2016, 138, 7248-7251.
TPH-Se	PBDB-TS1	8.52	0.56 ±0.01	0.90 ±0.04	16.53 ±0.26	Chem. Mater. 2019, 31, 3636−3643.
aFTTN-PDI4	P3TEA	8.6	0.61	1.17	12	J. Mater. Chem. A, 2019, 7, 8136-8143.
TPH	PBDB-TF	8.65	0.62	1.04	13.42	Chem. Mater. 2019, 31, 3636−3643.
FSP	PTB7-Th	8.89	59.5	0.9	16.6	ACS Appl. Mater. Interfaces, 2017, 9, 29924-29931.
TPH-Se	PBDB-T	9.05	0.70 ±0.01	0.939 ±0.003	13.41 ±0.11	Chem. Mater. 2019, 31, 3636−3643.
Ta-PDI	PTB7-Th	9.15	0.685	0.78	17.1	Adv. Mater. 2017, 29, 1605115.

TPH-Se	PDBT-T1	9.28	0.715	1	12.99	J. Am. Chem. Soc. 2016, 138, 10184-10190.
SF-PDI2	P3TEA	9.5	0.643	1.11	13.27	Nat. Energy 2016, 1, 16089.
BPT-Se1	PDBT-T1	9.54	0.732	1.06	12.3	Adv. Sci. 2019, 1802065.
Alq_3-PDI2	PTTEA	9.54	0.713	0.85	15.74	Adv. Funct. Mater. 2019, 1902079.
TPH-Se	PBDB-TF	9.63	0.64	1.057	14.23	Chem. Mater. 2019, 31, 3636−3643.
FTTB-PDI4	P3TEA	10.6	0.659	1.13	13.8	J. Am. Chem. Soc. 2017, 139, 16092-16095.

10. Computational Details for Intramolecular Charge Trap

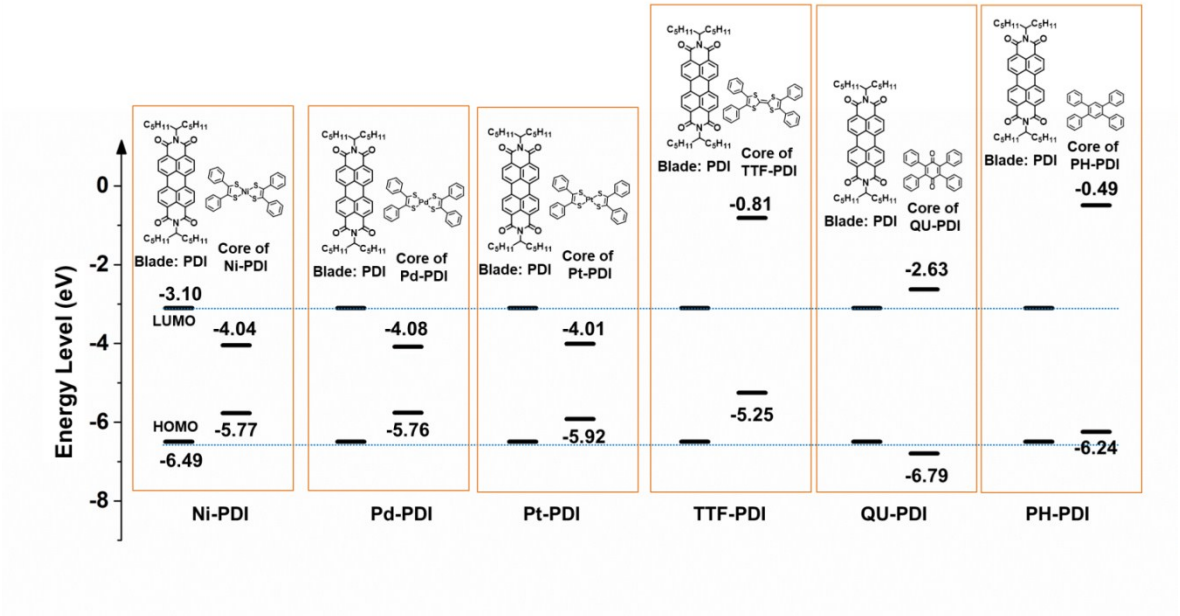

Figure S51. The detailed schematic diagram of intramolecular charge trap in six four-bladed PDI propellers with d^8 metal and non-metal cores. Density functional theory (DFT) calculations were performed using hybrid BLYP35 functional and 6-31G* basis set for C, H, O, N, the double-ξ quality LANL2DZ basis set and the Los Alamos effective core potentials for S, Ni, Pd, Pt[4, 5].

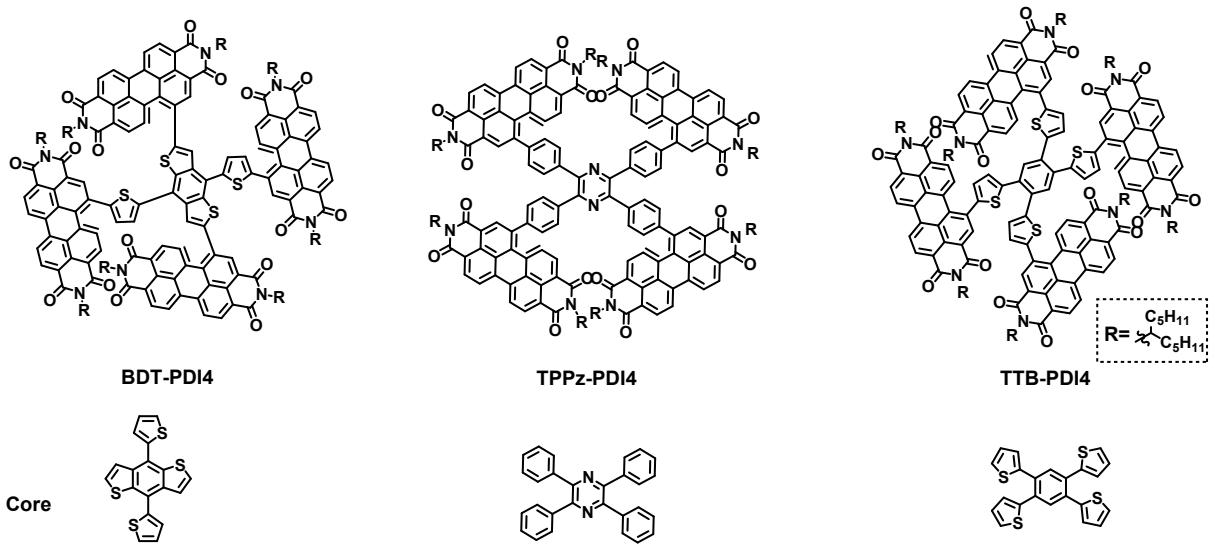

Figure S52. The detailed structures of reported four-bladed PDI propeller acceptors for comparisons in Table 6. TPPz-PDI4 in reference: *Adv. Mater.* 2016, *28*, 8546-8551. BDT-PDI4 and TTB-PDI4 in reference: *Adv. Energy Mater.* 2018, 1800234.

11. Supplemental References

1. P. Rajasingh, R. Cohen, E. Shirman, L. J. W. Shimon and B. Rybtchinski, *J. Org. Chem.*, 2007, **72**, 5973-5979.
2. T. T. Nguyen, D. Turp, D. Wang, B. Nolscher, F. Laquai and K. Mullen, *J. Am. Chem. Soc.*, 2011, **133**, 11194-11204.
3. G. Schrauzer and V.-P. Mayweg, *J. Am. Chem. Soc.*, 1965, **87**, 1483-1489.
4. D. G. Branzea, F. Pop, P. Auban-Senzier, R. Clerac, P. Alemany, E. Canadell and N. Avarvari, *J. Am. Chem. Soc.*, 2016, **138**, 6838-6851.
5. M. Renz, K. Theilacker, C. Lambert and M. Kaupp, *J. Am. Chem. Soc.*, 2009, **131**, 16292-16302.
6. I. S. Amiinu, Z. Pu, X. Liu, K. A. Owusu, H. G. R. Monestel, F. O. Boakye, H. Zhang and S. Mu, *Adv. Funct. Mater.*, 2017, **27**, 1702300.
7. H. J. Qiu, Y. Ito, W. Cong, Y. Tan, P. Liu, A. Hirata, T. Fujita, Z. Tang and M. Chen, *Angew. Chem. Int. Ed. Engl.*, 2015, **54**, 14031-14035.
8. T. B. K. Nørskov, A. Logadottir, J. R. Kitchin, J. G. Chen, S. Pandelov, U. Stimming, *J. Electrochem. Soc.*, 2005, **152**, J23-J26.
9. Y. Liu, G. Yu, G. D. Li, Y. Sun, T. Asefa, W. Chen and X. Zou, *Angew. Chem. Int. Ed. Engl.*, 2015, **54**, 10752-10757.
10. G. G. Liu, T. Koch, Y. Li, N. L. Doltsinis and Z. H. Wang, *Angew. Chem. Int. Edit.*, 2019, **58**, 178-183.
11. Y. Mitamura, H. Yorimitsu, K. Oshima and A. Osuka, *Chem. Sci.*, 2011, **2**, 2017-2021.
12. I. Ullah, R. A. Khera, M. Hussain, A. Villinger and P. Langer, *Tetrahedron Lett.*, 2009, **50**, 4651-4653.
13. T.-T. Bui, B. Garreau-de Bonneval and K. I. Moineau-Chane Ching, *New J. Chem.*, 2010, **34**, 337-347.
14. B. Garreau-de Bonneval, K. I. Moineau-Chane Ching, F. Alary, T.-T. Bui and L. Valade, *Coord. Chem. Rev.*, 2010, **254**, 1457-1467.
15. S. Debnath, H. F. Srour, B. Donnio, M. Fourmigué and F. Camerel, *Rsc Adv.*, 2012, **2**, 4453.
16. T. M. Vuong, T. T. Bui, A. Sournia-Saquet, A. Moreau and K. I. Ching, *Inorg. Chem.*, 2014, **53**, 2841-2847.
17. D. Zhu, X. Bao, Q. Zhu, C. Gu, M. Qiu, S. Wen, J. Wang, B. Shahid and R. Yang, *Energy Environ. Sci.*, 2017, **10**, 614-620.
18. X. Wang, Z. Du, K. Dou, H. Jiang, C. Gao, L. Han and R. Yang, *Adv. Energy Mater.*, 2019, **9**, 1802530.
19. X. Wang, K. Dou, B. Shahid, Z. Liu, Y. Li, M. Sun, N. Zheng, X. Bao and R. Yang, *Chem. Mater.*, 2019, **31**, 6163-6173.